processes

MDPI

Article

A Detailed Process and Techno-Economic Analysis of Methanol Synthesis from H_2 and CO_2 with Intermediate Condensation Steps

Bruno Lacerda de Oliveira Campos *, Kelechi John, Philipp Beeskow, Karla Herrera Delgado *, Stephan Pitter, Nicolaus Dahmen and Jörg Sauer

Institute of Catalysis Research and Technology (IKFT), Karlsruhe Institute of Technology (KIT), Hermann-von Helmholtz-Platz 1, D-76344 Eggenstein-Leopoldshafen, Germany
* Correspondence: bruno.campos@kit.edu (B.L.d.O.C.); karla.herrera@kit.edu (K.H.D.)

Abstract: In order to increase the typically low equilibrium CO_2 conversion to methanol using commercially proven technology, the addition of two intermediate condensation units between reaction steps is evaluated in this work. Detailed process simulations with heat integration and techno-economic analyses of methanol synthesis from green H_2 and captured CO_2 are presented here, comparing the proposed process with condensation steps with the conventional approach. In the new process, a CO_2 single-pass conversion of 53.9% was achieved, which is significantly higher than the conversion of the conventional process (28.5%) and its equilibrium conversion (30.4%). Consequently, the total recycle stream flow was halved, which reduced reactant losses in the purge stream and the compression work of the recycle streams, lowering operating costs by 4.8% (61.2 M€·a^{-1}). In spite of the additional number of heat exchangers and flash drums related to the intermediate condensation units, the fixed investment costs of the improved process decreased by 22.7% (94.5 M€). This was a consequence of the increased reaction rates and lower recycle flows, reducing the required size of the main equipment. Therefore, intermediate condensation steps are beneficial for methanol synthesis from H_2/CO_2, significantly boosting CO_2 single-pass conversion, which consequently reduces both the investment and operating costs.

Keywords: methanol synthesis; CO_2 utilization; power-to-X; intermediate condensation steps; product removal; techno-economic analysis; heat integration; plant simulation

check for updates

Citation: Lacerda de Oliveira Campos, B.; John, K.; Beeskow, P.; Herrera Delgado, K.; Pitter, S.; Dahmen, N.; Sauer, J. A Detailed Process and Techno-Economic Analysis of Methanol Synthesis from H_2 and CO_2 with Intermediate Condensation Steps. *Processes* **2022**, *10*, 1535. https://doi.org/10.3390/pr10081535

Academic Editors: Elio Santacesaria, Riccardo Tesser and Vincenzo Russo

Received: 13 July 2022
Accepted: 3 August 2022
Published: 5 August 2022

Publisher's Note: MDPI stays neutral with regard to jurisdictional claims in published maps and institutional affiliations.

Copyright: © 2022 by the authors. Licensee MDPI, Basel, Switzerland. This article is an open access article distributed under the terms and conditions of the Creative Commons Attribution (CC BY) license (https://creativecommons.org/licenses/by/4.0/).

1. Introduction

Sustainable solutions are required to reduce the greenhouse gas emissions of the transportation and industrial sectors, shrinking the dependency on fossil fuels. With the continuously increasing installed capacity of wind and solar power plants [1], adequate energy storage solutions have to be implemented in order to deal with their fluctuating nature. Therefore, the conversion of electricity into valuable chemicals and fuels, a concept often called power-to-fuels or power-to-X, can make an important contribution to the future energy system [2]. In this context, key process steps are hydrogen generation via electrolysis (primary conversion) [3,4] and methanol synthesis (secondary conversion) [5].

Methanol can be used as a fuel substitute or additive, either in fuel cells or via combustion [2], as a feedstock in the production of base chemicals (e.g., formaldehyde) and liquid fuels (e.g., gasoline, oxymethylene ethers, jetfuel) [6–8], and also as a solvent. Methanol fuel has recently attracted significant interest, especially in China, where the consumption of methanol for thermal applications (e.g., boilers, kilns, cooking stoves) and in the transportation section amounted to 5.7 Mton·a^{-1} (year 2019) [9].

The current global capacity of methanol production is 164 Mton·a^{-1} (year 2021), with an annual increase of 10% projected for the next decade [10]. Traditionally, methanol synthesis is fed by fossil-based syngas, which comes either from steam reforming of natural gas or from coal gasification [11]. However, sustainable syngas production is gaining

importance, such as from renewable electricity and captured CO_2, and also from biomass. In Figure 1, a scheme is presented showing the intermediate position of methanol in the conversion of both fossil-based and sustainable syngas to added-value chemicals and fuels, as well as methanol end-use applications.

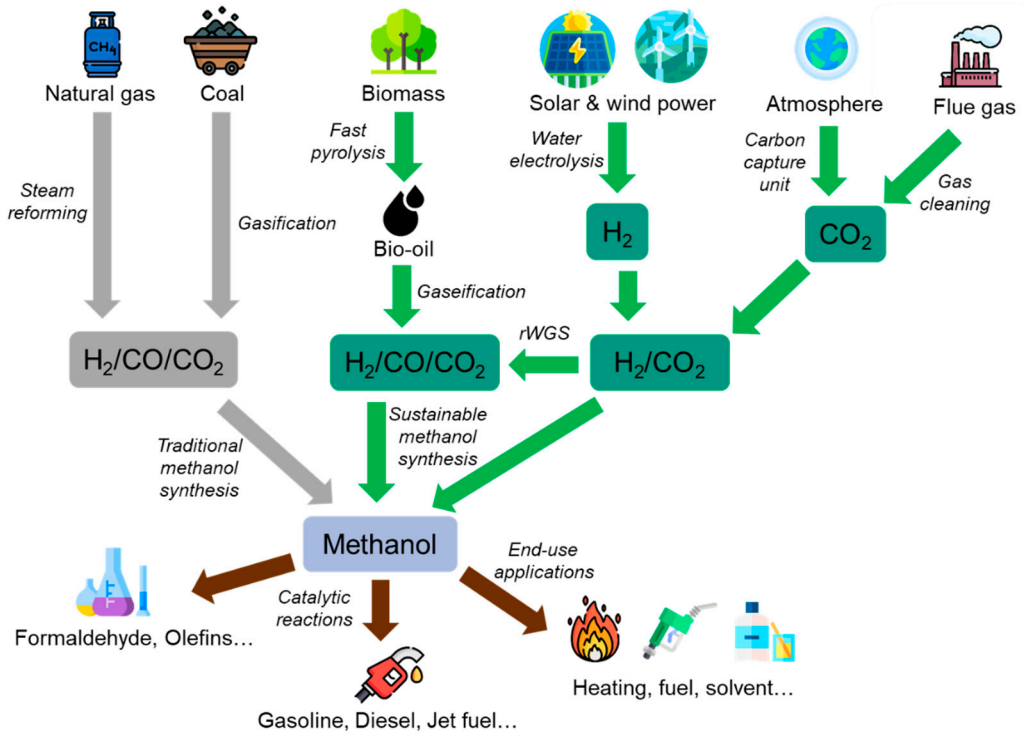

Figure 1. The key position of methanol to convert syngas sources into added-value chemicals and fuels. Icons from: Freepik, Flaticon [12].

The current world-scale technology for methanol synthesis is mostly based on the application of $Cu/ZnO/Al_2O_3$ (CZA) catalysts in either multi-tube reactors with boiling water as the cooling fluid, normally called isothermal reactors (e.g., the Lurgi process, the Linde process), or adiabatic reactors with intermediate cold syngas quenching, generally named quench reactors (e.g., ICI and the Casale process, the Haldor Topsoe process) [11,13]. Less common but also industrially applied are the adiabatic reactors with intermediate cooling (e.g., the Kellogg process, the Toyo process) [11,14]. Normally, temperatures between 200 and 300 °C and pressures between 50 and 100 bar are applied [13].

Methanol can be produced from either CO (Equation (1)) or CO_2 (Equation (2)), with the reverse water–gas shift reaction (rWGSR, Equation (3)) also occurring. If the feed gas contains both CO and CO_2, there is a prevailing opinion that direct CO hydrogenation (Equation (1)) on Cu/Zn-based catalysts is significantly slower than CO_2 hydrogenation [15,16], and kinetic models not considering this reaction can adequately simulate experimental data [17–19].

$$CO_{(g)} + 2{\cdot}H_{2(g)} \rightleftarrows CH_3OH_{(g)} \qquad \Delta H^0_{25\,^\circ C} = -90.6\ \text{kJ}{\cdot}\text{mol}^{-1} \tag{1}$$

$$CO_{2(g)} + 3{\cdot}H_{2(g)} \rightleftarrows CH_3OH_{(g)} + H_2O_{(g)} \qquad \Delta H^0_{25\,^\circ C} = -49.4\ \text{kJ}{\cdot}\text{mol}^{-1} \tag{2}$$

$$CO_{2(g)} + H_{2(g)} \rightleftarrows CO_{(g)} + H_2O_{(g)} \qquad \Delta H^0_{25\,^\circ C} = 41.2\ \text{kJ}{\cdot}\text{mol}^{-1} \tag{3}$$

With regard to the general use of CO_2 as a carbon source, several process simulations and techno-economic analyses of methanol synthesis from green hydrogen and captured CO_2 have been reported, with the CO_2 source being either a cleaned industrial flue gas or concentrated atmospheric CO_2 (i.e., through carbon capture units, CCUs) [20–22]. Pérez-Fortes et al. [20] and Szima et al. [21] simulated a methanol synthesis plant with CZA,

having a total production of 440 and 100 kton MeOH·a^{-1}, respectively. Heat integration was considered in both studies, with the plant being energetically self-sufficient. Cordero-Lanzac et al. [22] simulated the production of 275 kton MeOH·a^{-1} with an In_2O_3/Co catalyst. In all studies, it was concluded that economic viability can be achieved if reactant prices significantly decrease or if CO_2 taxation is enforced. Nonetheless, it is expected that the costs of electrolysis and CCUs might considerably decrease in the foreseeable future [23,24], and the first industrial-scale plants to produce e-methanol and e-gasoline are expected to start operating in 2024–2025 [25,26].

A general argument is the thermodynamic restrictions of CO_2 conversion to methanol compared to CO conversion (see Figure 2), whereby only limited methanol yields are achievable even at elevated pressures and lower temperatures. Consequently, a low CO_2 single-pass conversion ($X_{CO_2,SP}$) is obtained independently of the reactor size, leading to large recycle streams, which increase operating costs and cause higher reactant losses in purge streams.

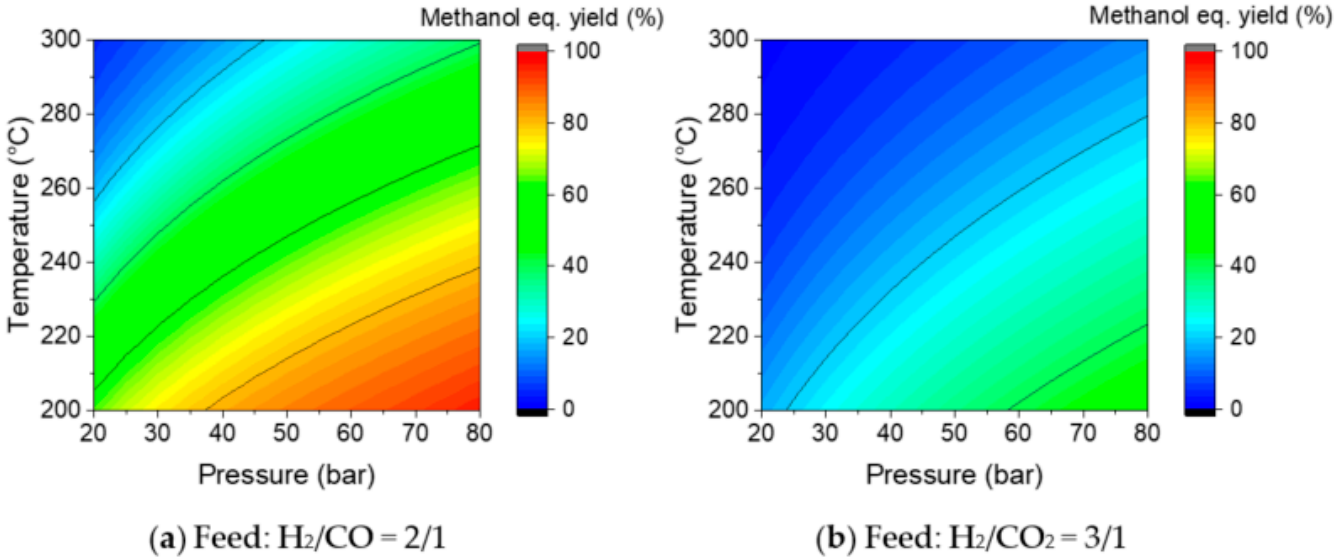

Figure 2. Methanol equilibrium yield as a function of temperature and pressure. Data generated with Aspen Plus. (**a**) H_2/CO feed in a 2:1 ratio. (**b**) H_2/CO_2 feed in a 3:1 ratio.

If the products (i.e., methanol and water) are removed from the reacting system, the thermodynamic equilibrium is shifted towards a higher methanol yield. This strategy has been studied using alternative reactor designs with in situ condensation [27,28] or membrane reactors [29], but these technologies are not yet ready for commercialization. A feasible approach using commercially proven technology is the implementation of intermediate condensation steps between reactor units displaced in series. In the Davy series loop methanol process, two reactors with an intermediate condensation unit are proposed for large scale methanol production from CO-rich syngas [13,30]. Although the implementation of intermediate condensation steps is a promising strategy to increase methanol yield from H_2/CO_2 syngas, such an approach has still not received particular attention, and plant simulations with heat integration and techno-economic analyses are not available in the literature yet, to the best of our knowledge.

In this work, the conventional approach (named here the 'one-step process') is compared with a new alternative approach including two condensation steps (named here the 'three-step process'). Using our recently developed kinetic model for methanol synthesis [19], both processes were implemented in Matlab in order to critically analyze and select key process parameters (i.e., cooling fluid temperature, number of reactor modules, and purge fraction). With the optimized parameters, detailed methanol synthesis plants with heat integration were implemented in Aspen Plus, and techno-economic analyses were performed.

2. Methodology

2.1. Process Overview

In the present work, a methanol synthesis plant from H_2/CO_2 with a production of 145 ton·h^{-1} is considered. This value is based on an ongoing power-to-gasoline project via H_2/CO_2 conversion to methanol [26], whose final goal is a gasoline production of $5.5 \cdot 10^8$ L·a^{-1}, which corresponds to a methanol production of 1.16 Mton·a^{-1} or 145 ton·h^{-1} (assuming a yield of 80% in the methanol-to-gasoline process and plant operating hours of 8000 h·a^{-1}).

In our simulations, feed carbon dioxide comes from the cleaned flue gas of nearby industries (e.g., a cement industry) at 25 °C and 1 bar, with a purity of 99.5% mol/mol (the rest was water). Feed hydrogen comes from water electrolysis at 25 °C and 30 bar, with a purity of 99.5% mol/mol (the rest was nitrogen). Although it is possible to obtain these feedstocks in an extremely high purity (e.g., 99.99% mol/mol) [31,32], we chose a more conservative scenario, which also allows a proper simulation of inert material accumulation in the plant.

As pressure has a significant influence on the thermodynamic equilibrium of methanol synthesis (see Figure 2), the reactor operating pressure was set to 70 bar. Although higher pressures are reported to have potential in methanol synthesis [33,34], they were out of the scope of this work, since considerable extrapolations in the kinetic model would be necessary, and condensation inside the reactor might have to be taken into account. Besides, higher pressures increase compression costs and might also require more expensive materials to build the equipment.

The dimensions of the reactor modules were chosen to be close to the upper size limits that are currently commercially available. That is, each reactor module consisted of a shell containing 33,000 tubes with 12.5 m length and an inner diameter of 3.75 cm. Since the heat generation in CO_2 hydrogenation is lower than in CO hydrogenation (Equations (1) and (2)), less heat transfer area is necessary. Because of that, the tube inner diameter chosen in this work (3.75 cm) was larger than the size typically used for CO conversion to methanol (2.5 cm). Considering 1050 kg·m^{-3} as the apparent catalyst bed density [35], the total CZA catalyst loading of each reactor module was 478.13 ton. A total pressure loss of 0.75 bar was considered for each reactor module [36].

2.1.1. One-Step Approach—Process Description

In Figure 3, a detailed flowsheet of the one-step process is presented. This is an adapted version from a concept reported in the literature [37–39]. Feed CO_2 is mixed with a low-pressure recycle stream, and then compressed from 1 to 70 bar in a three-stage process, including intermediate cooling (reducing compression work) and intermediate phase separation (to remove condensed methanol and water from the recycle stream). The resulting compressed stream is mixed with feed H_2 (compressed from 30 to 70 bar in one stage) and with a high pressure recycle stream. The mixed stream is preheated with the product gas and enters the inner tubes of parallel reactor modules, with the temperature being controlled by boiling water on the shell side.

The product stream is cooled down to 30 °C in four heat exchangers, condensing water, methanol, and some CO_2, which are separated from the light gases in a flash drum. A fraction of the gas stream is purged, and the remaining stream is recompressed to 70 bar and recycled. The liquid stream from the flash drum is depressurized to 1 bar and heated to 30 °C, vaporizing most remaining CO_2. A liquid–gas separation is performed in another flash drum. A fraction of the gas stream from the low-pressure flash drum is purged, and the rest is recycled by mixing with feed CO_2. The liquid stream from the low-pressure flash drum is preheated and fed to a packed column, where methanol in high purity (>99.5% m/m) is recovered in the liquid distillate, water is recovered in the bottom, and most of the remaining CO_2 is recovered in the gas distillate.

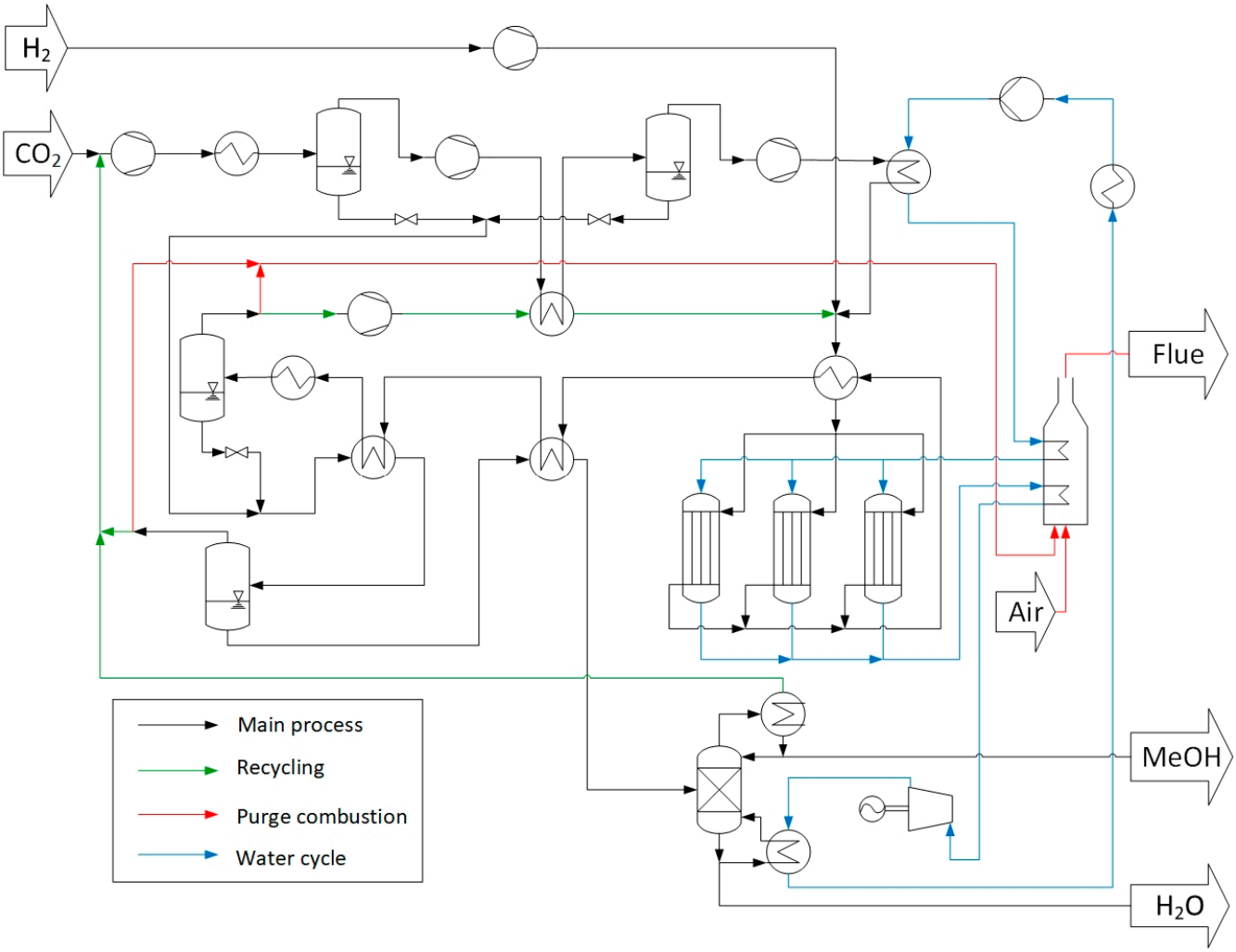

Figure 3. One-step process—detailed flowsheet with a total of three reactor modules. Cooling water streams are omitted.

The purge streams are burned with 15% air excess in a fired heater [40]. The heat of reaction of both the purge combustion and the methanol synthesis are used in a water Rankine cycle to produce electricity. The cycle starts with liquid water at 1 bar and 99.6 °C being pumped to a certain pressure, whose boiling temperature corresponds to the desired reactor temperature. Pressurized water reaches its boiling temperature in two steps (heat exchanger and fired heater) and vaporizes inside the reactor modules. The produced saturated steam is further heated in the fired heater and then performs work in a turbine, with a discharge pressure of 1.43 bar ($T_{boiling}$ = 110 °C). The resulting low-pressure steam condenses partially in the column reboiler, and total condensation is completed in a heat exchanger, closing the water cycle.

2.1.2. Three-Step Approach—Process Description

In Figure 4, a detailed flowsheet of the three-step process is presented. In this approach, the feed compression and recycling of non-converted reactants occurs similarly to the one-step process. The mixed feed stream is preheated and enters the first reactor module. The product gas is cooled down to 45 °C in three steps, and the condensed stream (mostly water, methanol, and some CO_2) is separated from the light gases in a flash drum. The gas stream is preheated and enters the second reactor module. The second product gas is cooled down to 30 °C in three steps, and the condensed stream (mostly water, methanol, and some CO_2) is separated from the gas stream in another flash drum.

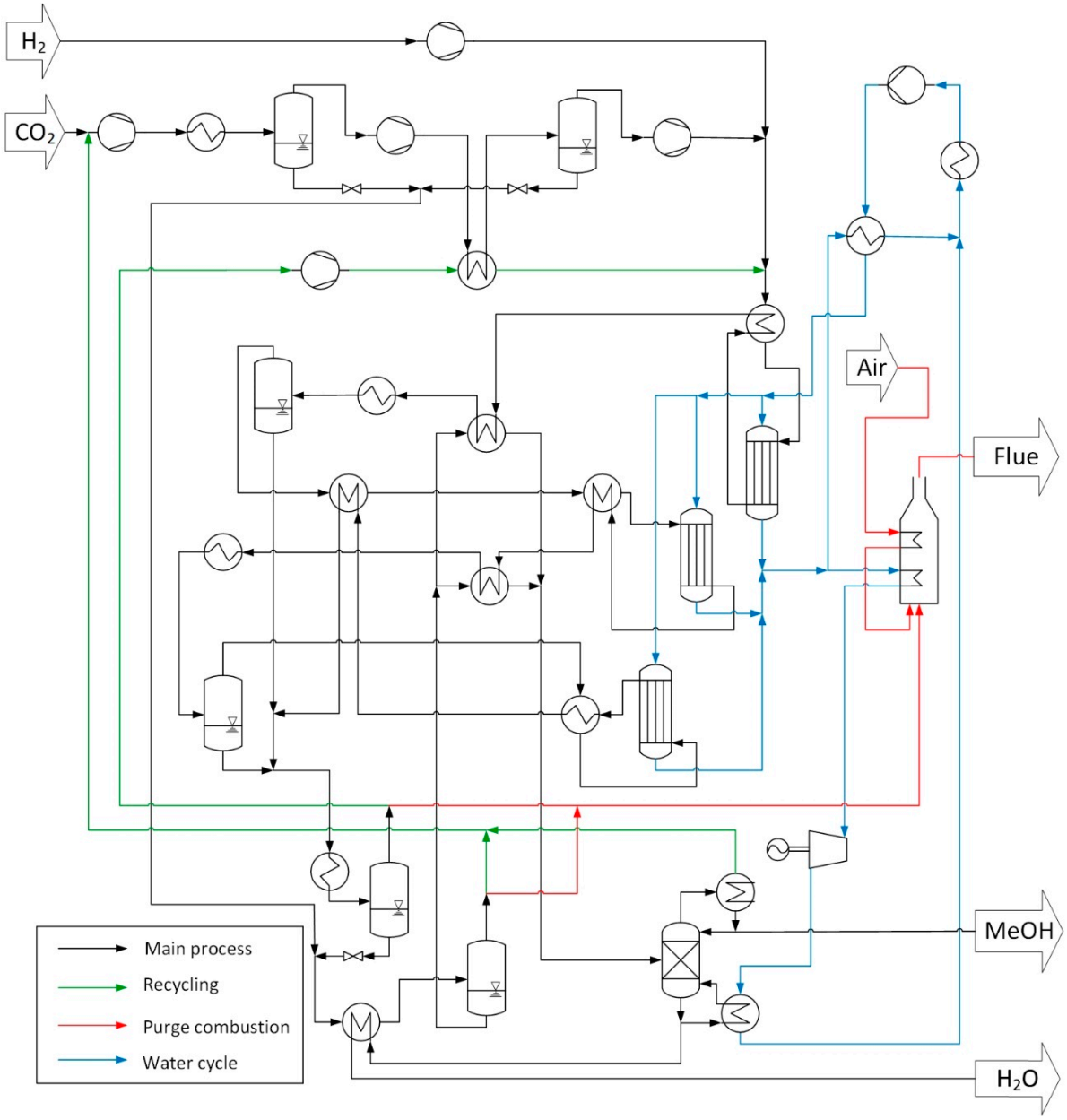

Figure 4. Three-step process—detailed flowsheet with a total of three reactor modules. Cooling water streams are omitted.

The gas phase is preheated and enters the third reactor module. The third product gas is cooled down, mixed with the condensed streams from the first and second reaction stages, and further cooled down to 30 °C.

Similar to the one-step process, component separation of the product stream is performed with one flash drum at high pressure, one flash drum at ambient pressure, and one distillation column.

The purge stream is burned in a fired heater with preheated air. In the water cycle, pressurized water is preheated and distributed to the reactor modules. A fraction of the produced saturated steam is split and used to preheat the water while the remaining steam is further heated in the fired heater. Supersaturated steam performs work in a turbine, with a discharge pressure of 1.43 bar ($T_{boiling}$ = 110 °C). The resulting low-pressure steam is partially condensed in the column reboiler, and total condensation is completed in a heat exchanger, closing the water cycle.

2.2. Process Simulation in Matlab

Before implementing the final version of each plant in Aspen Plus, different scenarios were investigated in Matlab. Therefore, optimal key parameters were selected, such as the total number of reactor modules, the purge fraction, and the temperature of the cooling fluid in the reactor.

In order to simulate the reactor, the following considerations were made: there are only variations along the length of the reactor (1D assumption), the influence of back-mixing is neglected (plug flow assumption), and the cooling fluid temperature (T_w, in K) is constant. Starting from mass and energy balances, the differential equations of the total mole flow of a single tube ($\dot{n}$, in mol·s^{-1}), the mole fraction of each component j (y_j), and the temperature (T, in K) in the axial direction z are shown as follows:

$$\frac{d\dot{n}}{dz} = \frac{m_{Cat}}{L} \cdot \sum_{j=1}^{6} \sum_{k=1}^{2} (\nu_{jk} \cdot r_k) \tag{4}$$

$$\frac{dy_j}{dz} = \frac{1}{\dot{n}} \cdot \left\{ \frac{m_{Cat}}{L} \cdot \sum_{k=1}^{2} (\nu_{jk} \cdot r_k) - y_j \cdot \frac{d\dot{n}}{dz} \right\} \tag{5}$$

$$\frac{dT}{dz} = \frac{1}{\left(\dot{n} \cdot C_{P,f}\right)} \cdot \left[-\frac{d\dot{n}}{dz} \cdot h_f - \dot{n} \cdot \sum_{j=1}^{6} \left(h_j \cdot \frac{dy_j}{dz} \right) + U \cdot \pi \cdot D_i \cdot (T_w - T) \right] \tag{6}$$

where m_{Cat} is the catalyst mass (kg), L is the reactor length (m), y_{jk} is the stoichiometric coefficient of component j in reaction k, r_k is the rate of reaction k (mol·kg$_{cat}$·s^{-1}), $C_{P,f}$ is the heat capacity of the fluid (J·mol·K^{-1}), h_f is the specific enthalpy of the fluid (J·mol^{-1}), h_j is the specific enthalpy of component j, U is the global heat transfer coefficient (W·m^{-2}·K^{-1}), and D_i is the inner diameter of a single tube (m).

The temperature-dependent parameters ($C_{P,f}$, h_f, h_j, U) were updated in each integration point in the axial direction. Heat capacity and enthalpy were calculated with the thermodynamic functions provided by Goos et al. [41], which are detailed in the Supplementary Material (Section A) along with the derivation of the differential equations. The global heat transfer coefficient was estimated (U) by summing the heat transfer resistances in the axial direction, according to the methodology described in the literature [42,43] (see Section B of the Supplementary Material).

The methodology to calculate the reaction rates (r_k) is described in Section 2.3. The system of differential equations was solved with the Matlab function ode45, with absolute and relative tolerances set to 10^{-10}.

In order to simplify the simulation of the separation steps in Matlab, the following procedure was applied. Both processes were implemented in Aspen Plus, considering a total of six reactor modules, a purge fraction of 2%, and T_w = 235 °C. The values of the split ratio of each component in the liquid and gas phase of each flash drum and the distillation column were extracted. For example, in the column of the one-step process, the methanol distribution in the outlet streams was: 3.80% in the gas distillate, 96.13% in the liquid distillate, and 0.06% in the bottom. The split ratio of all the components were taken from Aspen Plus and were considered constant for the different scenarios investigated in Matlab (i.e., variations in the number of reactor modules, purge fraction, and T_w). These split ratios are provided in the Supplementary Material (Section C).

Flowsheet convergence was achieved in Matlab by an iterative method, as there were two cycles of streams due to recycling unconverted reactants. First, educated initial guesses of the composition and total mole flow of each recycle stream were given. In each iteration, the recycle stream mole flow and its composition were calculated and used in the next iteration until the tolerance criterion was fulfilled:

$$\frac{\left(\dot{n}_{Ref,k+1} - \dot{n}_{Ref,k}\right)^2}{\left(\dot{n}_{Ref,k+1}\right)^2} \leq Tolerance \tag{7}$$

where $\dot{n}_{Ref,k}$ is the total mole flow of the recycle stream at iteration k. The tolerance of the inner cycle and the outer cycle were set to 10^{-9} and 10^{-8}, respectively.

2.3. Kinetic Modeling of the Methanol Synthesis

The kinetic simulation of the methanol synthesis was performed with our previously published six-parameter model (Model-6p) [19], whose considerations regarding the reaction mechanism, the assumption of the rate determining steps, and the most abundant surface species were based on our detailed microkinetic model [15]. This six-parameter model was validated with 496 experimental points from different laboratory plants [15,18,44], which contemplated temperatures between 210 and 260 °C, pressures between 20 and 60 bar, gas hourly space velocities (GHSV) between 1.8 and 40 $L_S \cdot h^{-1} \cdot g_{cat}{}^{-1}$, and a variety of syngas ($H_2/CO/CO_2/N_2$) feed compositions, including 126 points with only $H_2/CO_2/N_2$ in feed.

In this model, two main reactions are considered: CO_2 hydrogenation (Equation (2)) and the rWGSR (Equation (3)). The reaction rates ($r_{CO_2\ hyd.}$, r_{rWGSR}) in $mol \cdot kg_{cat}{}^{-1} \cdot s^{-1}$ are described as follows:

$$r_{CO_2\ hyd.} = \exp\left(A_2 - \frac{E_{A,2}}{R \cdot T}\right) \cdot \phi_{Zn} \cdot \theta_b \cdot \theta_c \cdot f_{H_2}^{1.5} \cdot f_{CO_2} \cdot \left(1 - \frac{f_{CH_3OH} \cdot f_{H_2O}}{f_{H_2}^3 \cdot f_{CO_2} \cdot K^0_{P,CO_2\ hyd.}}\right) \tag{8}$$

$$r_{rWGSR} = \exp\left(A_3 - \frac{E_{A,3}}{R \cdot T}\right) \cdot \phi_{Zn} \cdot \theta_b \cdot \theta_c \cdot f_{CO_2} \cdot f_{H_2O} \cdot \left(1 - \frac{f_{CO} \cdot f_{H_2O}}{f_{H_2} \cdot f_{CO_2} \cdot K^0_{P,rWGSR}}\right) \tag{9}$$

Here, A_{2-3} and $E_{A,2-3}$ are kinetic parameters, R is the universal gas constant, ϕ_{Zn} is the zinc coverage on the surface, θ_b and θ_c are the free active sites b and c, f_j is the fugacity of gas component j (bar), and $K^0_{P,k}$ is the global equilibrium constant of reaction k.

The Peng–Robinson equation of state is used to calculate the fugacities [45], considering the binary interaction parameters reported by Meng et al. [46] and Meng and Duan [47], and an effective hydrogen acentric factor of −0.05 proposed by Deiters et al. [48].

The zinc coverage is dependent on temperature and gas concentration [49], and its exact quantification under reaction conditions is difficult to predict. The zinc coverage is then considered to be constant and equal to ϕ_{Zn} = 0.50 for a general case, while it is set to ϕ_{Zn} = 0.10 for CO_2-rich feed (CO_2/CO_x > 0.90). The free active sites are calculated with the following equations:

$$\theta_b = \left(\overline{K_2} \cdot f_{H_2}^{0.5} \cdot f_{CO_2} + 1\right)^{-1} \tag{10}$$

$$\theta_c = \left(\overline{K_3} \cdot f_{H_2}^{-0.5} \cdot f_{H_2O} + 1\right)^{-1} \tag{11}$$

where $\overline{K_{2-3}}$ are adsorption parameters. In Table 1, the equilibrium constants as well as the previously estimated kinetic and adsorption parameters are summarized [19].

The side products of methanol synthesis on Cu/Zn-based catalysts (e.g., hydrocarbons or dimethyl ether) are typically at low concentrations [13,50]. Several studies reported that syngas conversion to hydrocarbons or dimethyl ether on commercial CZA at moderate temperatures (T ≤ 260 °C) is significantly low or even below detection range [15,18,44], while Condero-Lanzac et al. [22] reported low methane production from H_2/CO_2 on CZA at high temperatures (T ≥ 275 °C). Saito et al. [51] observed that side product formation is further reduced by increasing CO_2/CO_X feed concentration. Therefore, the generation of side products is not considered in this work.

Table 1. Equilibrium constants, kinetic and adsorption parameters of Model-6p [19]. Reprinted with permission from [19]. Copyright 2021 American Chemical Society.

Parameter	Value ǀ Equation	Unit
A_2	14.41 ± 0.99	–
A_3	29.13 ± 1.74	–
$E_{A,2}$	94.73 ± 4.18	$kJ \cdot mol^{-1}$
$E_{A,3}$	132.79 ± 7.46	$kJ \cdot mol^{-1}$
$\overline{K_2}$	0.1441 ± 0.0289	$bar^{-1.5}$
$\overline{K_3}$	49.44 ± 11.08	$bar^{-0.5}$
$K^0_{P,CO_2\ hyd.}$	$T^{-4.481} \cdot \exp\left(\frac{4755.7}{T} + 8.369\right)$	bar^{-2}
$K^0_{P,rWGSR}$	$T^{-1.097} \cdot \exp\left(\frac{-5337.4}{T} + 12.569\right)$	–

2.4. Process Analysis and Optimization

Considering the fixed methanol production of 145 $ton \cdot h^{-1}$ or 1257.1 $mol \cdot s^{-1}$ and the 99.5% mol/mol purity of the reactants, the minimum required feed is 1263.4 $mol \cdot s^{-1}$ of CO_2 and 3790.3 $mol \cdot s^{-1}$ of H_2, totalizing $\dot{n}_{feed,min}$ = 5053.7 $mol \cdot s^{-1}$. Since there are reactant losses in the purge and product streams, an excess of feed is required. With a fix feed ratio H_2:CO_2 of 3:1, the excess of feed (Exc) is defined here as:

$$Exc = \frac{\left(\dot{n}_{feed} - \dot{n}_{feed,min}\right)}{\dot{n}_{feed,min}} \cdot 100\% \quad (12)$$

It is, of course, of interest to minimize feed consumption, due to its high costs. Feed consumption is affected by key variables, such as reactor temperature and pressure, the number of reactor modules (which defines the total catalyst mass), and purge fraction. Avoiding large recycle streams is also important, as compressor work is required to get the pressure back to 70 bar, and larger equipment (i.e., heat exchangers, flash drums, compressors) are required to process higher flows.

Simulations were performed for a different number of reactor modules (from 3 to 12) and different purge fractions (from 0.5 to 5%). For each case, an initial guess for the feed excess was given (Exc = 5%), and a fix feed ratio H_2:CO_2 of 3:1 (a stoichiometric ratio) was applied. Then, an optimization problem was solved in Matlab with the function fminsearch (function tolerance = 0.1 $mol \cdot s^{-1}$, step tolerance = 0.1 °C), whose objective was to maximize methanol production by varying the reactor coolant temperature (T_w).

With the optimum T_w, the required excess of feed was calculated to meet the methanol demand (1257.1 $mol \cdot s^{-1}$) with Newton's method (function tolerance: 0.1 $mol \cdot s^{-1}$). The steps of the temperature optimization and Exc calculations were repeated until the temperature update was lower than 0.25 °C.

2.5. Detailed Plant Simulation in Aspen Plus

After analyzing the results of the Matlab simulations, optimum parameters were selected for each approach (i.e., the number of reactor modules, purge fraction, cooling fluid temperature) and a detailed plant simulation including heat integration was implemented in Aspen Plus V10.

The Peng–Robinson property method was selected for the reactor modules. All other equipment were simulated with the Non-Random Two-Liquid Model with a second set of binary parameters (NRTL2) as the property method.

The methanol synthesis reactor was simulated with the rigorous plug flow reactor model (RPLUG unit) and the kinetics described in Section 2.3 were implemented as a Langmuir–Hinshelwood–Hougen–Watson (LHHW) reaction model. The rearrangement of the model parameters to follow the software's specific input format is detailed in the Supplementary Material (Section D). Since the reactor cooling fluid is at a constant temperature due to water evaporation, both co-current and counter-current operations give

the same results. Therefore, the co-current operation was selected in order to simplify the mathematical calculations.

The combustion of the purge streams in a fired heater was simulated with the RGIBBS unit, which considers that chemical equilibrium is achieved when the free Gibbs energy of the system is minimized.

The heat exchangers were simulated in counter-current flow with the HeatX unit, with a minimum temperature approach of 25 °C for the heat exchangers located inside the fired heater and a minimum temperature approach of 10 °C for all the other heat exchangers.

The compressors were modeled using the ASME method, assuming a mechanical efficiency of 0.95 and an isentropic efficiency of 0.80 [22]. The pump was simulated assuming an efficiency of 0.70. The turbine was simulated with the ASME method, assuming a mechanical efficiency of 0.95 and an isentropic efficiency of 0.90 [52].

The distillation column was simulated with the rigorous RadFrac model, considering a kettle reboiler and a partial condenser at 53 °C with liquid and vapor distillate. A Murphree efficiency of 0.75 was set to all intermediate stages [53,54]. In both processes, the column had 30 stages and a reflux ratio of 2, with the feed entering above the 24th stage.

The relative tolerance of all equipment calculations was set to 10^{-5}. Flowsheet convergence was achieved using the Broyden method, with a relative tolerance of 10^{-4}, which corresponds to a mass balance closure of 99.99%.

2.6. Efficiency Evaluation

The chemical conversion efficiency (η_{CCE}) accounts for how much fuel energy remains in the final product in relation to the reactants. For methanol synthesis from H_2/CO_2, it is calculated as follows: [55]

$$\eta_{CCE} = \frac{\dot{m}_{MeOH} \cdot LHV_{MeOH}}{\dot{m}_{H_2} \cdot LHV_{H_2}} \tag{13}$$

where $\dot{m}_{MeOH}$ is the methanol mass production, $\dot{m}_{H_2}$ is the hydrogen feed demand, and LHV is the low heating value. The maximum possible efficiency ($\eta_{CCE,max}$) occurs at 100% overall H_2 conversion to methanol (stoichiometric conversion):

$$\eta_{CCE,max} = \frac{M_{MeOH} \cdot LHV_{MeOH}}{3 \cdot M_{H_2} \cdot LHV_{H_2}} = 0.876 \tag{14}$$

Here, M_j is the molar mass of component j. In order to also account for heat and the work input, the exergy efficiency (η_{Ex}) is calculated: [39]

$$\eta_{Ex} = \frac{\dot{m}_{MeOH} \cdot e_{MeOH}}{\dot{m}_{H_2} \cdot e_{H_2} + \dot{m}_{CO_2} \cdot e_{CO_2} + P_{el} + E_Q} \tag{15}$$

where e_j is the specific exergy of component j, P_{el} is the total required electric power, and E_Q is the total exergy input associated with heat demand.

The specific exergy of a component (e_j) is divided between thermal and chemical exergy: [39]

$$e_j(T,p) = \left[e_{j,therm}\right] + e_{j,chem} = \left[H_j - S_j \cdot T_0 - H_j^0 + S_j^0 \cdot T_0\right] + HHV_j \tag{16}$$

Here, $e_{j,therm}$ and $e_{j,chem}$ are the thermal and chemical exergies, H_j is enthalpy, S_j is entropy, H_j^0 and S_j^0 are the enthalpy and entropy at reference conditions (298.15 K and 1 bar), T_0 is the reference temperature, and HHV_j is the high heating value. In the exergy efficiency calculation, the HHV is used instead of the LHV, as water is liquid at reference conditions.

2.7. Techno-Economic Evaluation

In order to calculate the production costs, the standardized methodology from Albrecht et al. [56] was considered, which is a further development based on the work of Peters et al. [57].

The main equipment costs (EC) were estimated based on reference equipment costs [57,58]. The scale up to the required capacity was performed with specific equipment scaling factors, and price inflation was corrected to 2020 with the Chemical Engineering Plant Cost Indexes ($CEPCI$). In Equation (23), the costs of equipment j (EC_j) is described:

$$EC_j = EC_{j,ref} \cdot \left(\frac{C_j}{C_{j,ref}} \right)^M \cdot \left(\frac{CEPCI_{2020}}{CEPCI_{ref}} \right) \quad (17)$$

Here, the subscription ref relates to the reference equipment, C is the characteristic capacity, and M is the equipment scaling factor. The equipment is constructed with carbon steel. When the reference price is in US dollars (USD), a conversion to euros (EUR) of 1.13 USD·EUR^{-1} is applied (February 2022) [59].

The dimensions of the flash drums and the packed distillation column were calculated with the methodology reported by Towler and Sinnott [60]. The required heat transfer area of the heat exchangers, column condenser, and reboiler were estimated by assuming the typical global heat transfer coefficients reported by the VDI Atlas [43], according to each specific situation. Equipment dimensioning is detailed in the Supplementary Material (Section G).

The fixed capital investment (FCI) was estimated by multiplying the total EC with the Lang Factor (LF), which accounts for all direct and indirect costs related to the plant construction. In this work, LF was assumed to be 4.86 (details are provided in the Supplementary Material, Section H) [56,57]. A working capital (WC) of 10% of the total capital expenses ($CAPEX$) was considered [56]. Summarizing the equations:

$$FCI = LF \cdot \sum EC_j \quad (18)$$

$$CAPEX = FCI + WC \quad (19)$$

$$WC = 0.10 \cdot CAPEX \quad (20)$$

The equivalent annual capital costs (ACC) were estimated by applying the annuity method on the FCI, assuming an annual interest rate (IR) of 10%, a plant operating life (t_P) of 20 years, and no salvage value [61]. The working capital does not depreciate in value, and only its interest has to be taken into account [56].

$$ACC_{FCI} = \frac{FCI \cdot IR \cdot (1 + IR)^{t_P}}{[(1 + IR)^{t_P} - 1]} \quad (21)$$

$$ACC_{WC} = WC \cdot IR \quad (22)$$

$$ACC = ACC_{FCI} + ACC_{WC} = \frac{FCI \cdot IR \cdot (1 + IR)^{t_P}}{[(1 + IR)^{t_P} - 1]} + WC \cdot IR \quad (23)$$

The operating expenses ($OPEX$) were divided between direct and indirect costs. The costs related to the direct OPEX ($OPEX_{dir}$) are presented in Table 2, which include raw materials, catalysts, process water treating, and electricity. A catalyst lifetime of three years was considered. In the Rankine water cycle, a clean water replacement of 1% of the total flow was considered [62].

The indirect $OPEX$ consisted of operating labor (OL), operating supervision, maintenance, operating supplies, laboratory charges, taxes on property, insurance, plant overhead, administration, distribution, marketing, research, and development. The estimation of each of these items was based on typical values, which are dependent on OL, FCI, and the net production costs (NPC) (see Section H of the Supplementary Material) [56,57]. The total indirect $OPEX$ ($OPEX_{ind}$) is calculated as follows:

$$OPEX_{ind} = 2.2125 \cdot OL + 0.081 \cdot FCI + 0.10 \cdot NPC \quad (24)$$

Table 2. Costs of feedstock, catalyst, water treating, and electricity.

Item	Costs	Ref.
Hydrogen	3097.4 €·ton^{-1}	[22]
Carbon dioxide	44.3 €·ton^{-1}	[22]
Cooling water	0.00125 €·ton^{-1}	[56]
Clean water	2 €·ton^{-1}	[56]
Total organic carbon (TOC) abatement of process water	1938 €·(ton C)$^{-1}$	[63]
Electricity	90 €·MWh^{-1}	[53]
Catalyst ($Cu/ZnO/Al_2O_3$)	18,100 €·ton^{-1}	[64]

The required number of operators in a shift (n_{OP}) was estimated with the following equation: [65,66]

$$n_{OP} = (6.29 + 0.23 \cdot N_{np})^{0.5} \quad (25)$$

where N_{np} is the number of non-particulate main processing units. Considering daily working shifts, resting periods and vacations, the number of operators to fulfill each position in a continuous operation is approximately F_{OP} = 4.5. Therefore, the total number of operators (N_{OP}) is: [65,66]

$$N_{OP} = F_{OP} \cdot n_{OP} \quad (26)$$

The total costs of operating labor (OL) is then calculated as follows:

$$OL = W_{OP} \cdot N_{OP} \quad (27)$$

where W_{OP} is the wage rate of each operator (W_{OP} = 72,000 €·a^{-1}) [53].

The net production costs (NPC) are calculated in terms of average annual costs and in terms of average costs per kg of methanol:

$$NPC \left[\frac{€}{a}\right] = ACC + OPEX_{dir} + OPEX_{ind} \quad (28)$$

$$NPC \left[\frac{€}{kg}\right] = \frac{(ACC + OPEX_{dir} + OPEX_{ind})}{\dot{m}_{MEOH}} \quad (29)$$

3. Results and Discussion

In this section, process simulation and analysis are presented separately for the one-step and the three-step approaches. Finally, the techno-economic analysis of both approaches is presented and discussed jointly.

3.1. One-Step Process

3.1.1. One-Step Process—Selecting Key Parameters

The one-step process was successfully implemented in Matlab. Different scenarios were simulated by varying the number of reactor modules and the purge fraction, with the optimal temperature for a fixed methanol production (145 ton·h^{-1}) being estimated in each case. In Figure 5, several contour plots are shown, where CO_2 single-pass conversion ($X_{CO_2,SP}$) (Figure 5a), the required feed excess (Figure 5b), the optimal temperature (Figure 5c), and the total recycle stream (Figure 5d) are plotted against the number of reactor modules and the purge fraction.

CO_2 single-pass conversion (Figure 5a) was considerably enhanced by increasing the number of reactor modules. This was not only because the gas hourly space velocity (GHSV) decreased, but also because the optimal temperature had lower values (Figure 5c), shifting the thermodynamic equilibrium towards higher methanol concentrations. In contrast, reducing the purge fraction had little effect on $X_{CO_2,SP}$. This should be the result of two competing effects: on one hand, a lower purge fraction means higher recycle streams (Figure 5d), which increases the GHSV, reducing $X_{CO_2,SP}$. On the other hand, the recycle stream has a H_2:CO_2 ratio greater than three due to a limited rWGSR extension.

By increasing the recycle stream, the H_2:CO_2 ratio of the reactor feed stream is enhanced, positively contributing to $X_{CO_2,SP}$.

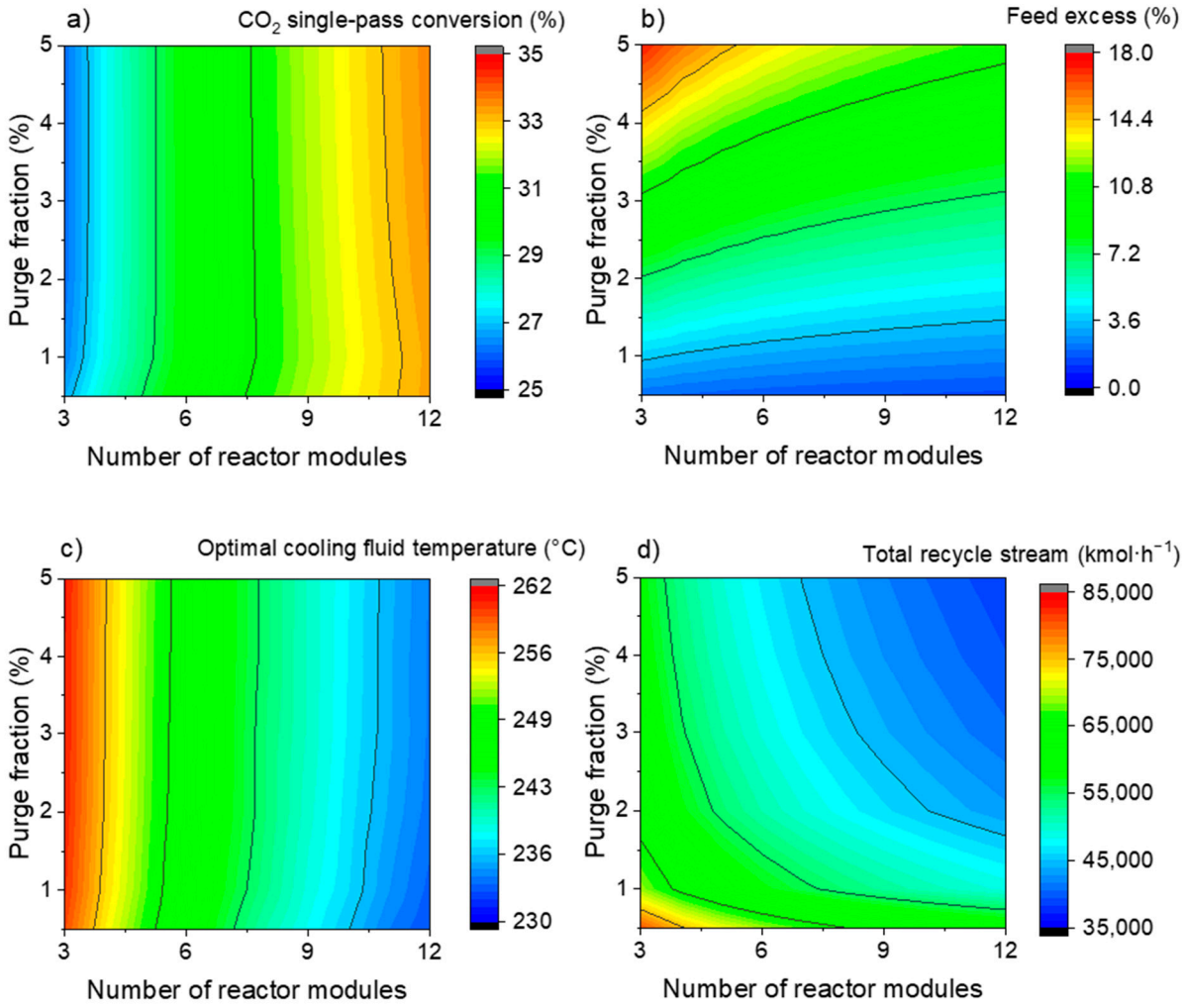

Figure 5. One-step process—CO_2 single-pass conversion (**a**), required feed excess (**b**), optimal temperature (**c**), and total recycle stream (**d**) as a function of the number of reactor modules and the purge fraction.

The required feed excess was significantly decreased both by increasing the number of reactor modules and by reducing the purge fraction. This occurred because the former procedure increased $X_{CO_2,SP}$ and the latter maintained $X_{CO_2,SP}$ roughly constant while increasing the gas flow inside the reactor modules.

Since the reactants (H_2, CO_2) represent the highest costs of the plant, it is important to minimize the required feed excess, which according to Figure 5b, occurred at 0.5% purge fraction. However, with such a low purge fraction, the total recycle stream was considerably high, demanding larger heat exchangers, flash drums, and compressors, as well as higher power consumption. Therefore, an intermediate value of 2% as the purge fraction was selected for the detailed simulation in Aspen Plus, agreeing with other studies and typical industrial values [22,39,58].

With the purge fraction fixed at 2%, six reactor modules were used in the detailed study, because further increasing the number of reactor modules only slightly reduced the required excess feed, not justifying further expenses in equipment and catalyst.

The value of the global heat transfer coefficient was updated point by point within mathematical integration along the reactor length. For the selected condition, $U_{z=0}$ = 160 W·m^{-2}·K^{-1}

and $U_{z=12.5}$ = 150 W·m^{-2}·K^{-1}. Since Aspen Plus requires a constant value, the average value was used (U_{avg} = 155 W·m^{-2}·K^{-1}).

3.1.2. One-Step Process—Detailed Plant Simulation and Process Analysis

A detailed flowsheet of the one-step process presented in Figure 3 was implemented in Aspen Plus, considering 2% purge fraction, six reactor modules working in parallel, and the optimized temperature of the reactor cooling fluid (T_w = 247.5 °C). A picture of the flowsheet in Aspen Plus, the properties of the streams, and a detailed plant description are provided in the Supplementary Material (Section E).

In Figure 6, the concentration of the products along the reactor length is shown. The methanol and water feed concentrations were close to zero, and their outlet concentrations were 7.4 and 7.2% mol/mol, respectively. The nitrogen concentration remained relatively low (inlet: 4.95% mol/mol, outlet: 5.65% mol/mol). Due to the recycle streams, CO entered the reactor modules at 1.50% mol/mol, although it was not a feedstock in the plant. CO was produced through the rWGSR until the length of 1.5 m, where its concentration reached 3.3% mol/mol. Then, due to the high water concentration (4.30% mol/mol), the WGSR became faster than its reverse reaction and started to consume CO, which exited the reactor at 1.76% mol/mol and a marginal selectivity (0.5%). This virtually stabilized CO content in the plant led to a high methanol selectivity (99.5%).

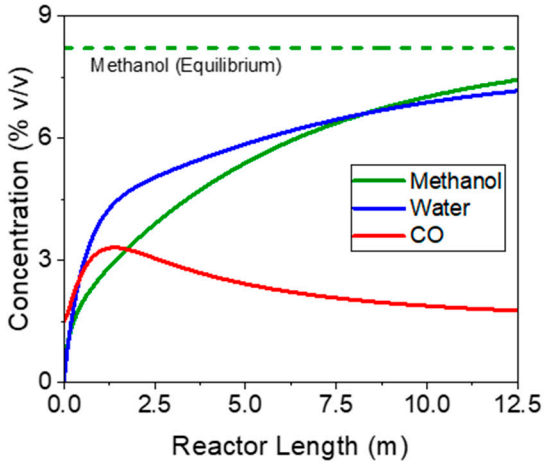

Figure 6. One-step process—product concentration along the reactor length. Reactor feed concentration: $H_2/CO/CO_2/CH_3OH/H_2O/N_2$ = 71.3/1.5/21.9/0.3/0.0/5.0% mol/mol.

The CO_2 single-pass conversion was 28.5%, close to the equilibrium conversion (30.4%), while the feed excess was 6.05%, which corresponded to an overall CO_2 conversion to methanol of 94.3%. These values are in agreement with the Matlab simulations ($X_{CO_2,SP}$ = 29.7%, feed excess = 5.75%, overall CO_2 conversion to MeOH = 94.6%).

The chemical conversion efficiency (η_{CCE}) of the process was 82.6%, which was close to the maximum possible value ($\eta_{CCE,max}$ = 87.6%). With the heat integration, the one-step process was not only self-sufficient, but had a heat excess that could be supplied to other processes, in agreement with the literature [21,39]. In our case, as is commonly performed in industrial methanol synthesis plants, the heat excess was used to generate electricity via a water Rankine cycle, reducing the electricity consumption from 47.4 to 17.6 MW.

In Figure 7, a global exergy balance and an exergy loss distribution are provided. No distinction was made between exergy destruction and exergy losses via side output streams (i.e., cooling water, process water, and flue gas). The exergy efficiency (η_{Ex}) of the process was 76.4%, with a total exergy loss of 281.9 MW. The main losses occurred due to the exothermic chemical reactions with heat recovery at low temperatures (reactor modules: 58.1%, fired heater: 14.8%). Additionally, exergy losses in the heat exchangers (11.1%) and in the column (9.0%) were also significant, mainly due to heat transfer to cooling water.

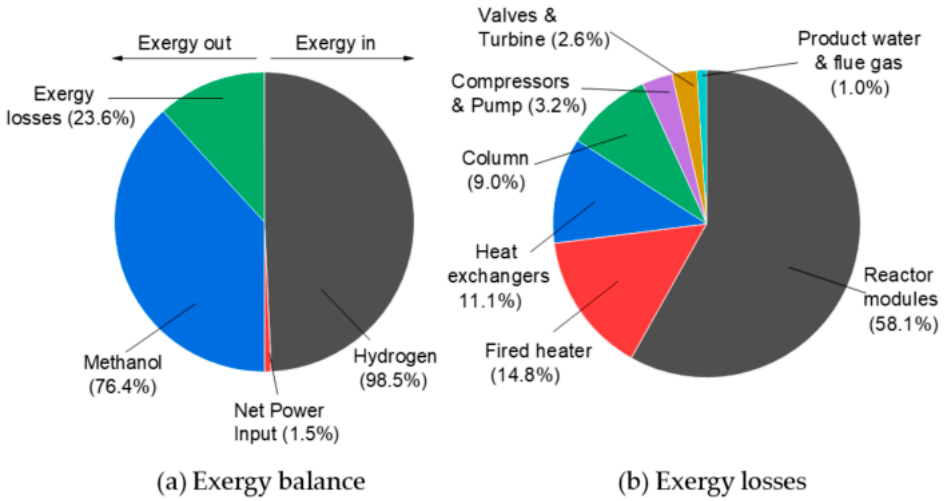

Figure 7. One-step process—exergy analysis. (**a**) Global exergy balance. Total exergy input: 1194.5 MW. (**b**) Distribution of exergy losses (total = 281.9 MW).

3.2. Three-Step Process

3.2.1. Three-Step Process—Selecting Key Parameters

The three-step process was successfully implemented in Matlab. In Figure 8, CO_2 single-pass conversion ($X_{CO_2,SP}$) (Figure 8a), the required feed excess (Figure 8b), the optimal temperature (Figure 8c), and the total recycle stream (Figure 8d) are described as a function of the number of reactor modules and the purge fraction. Since this process considers three reaction steps with intermediate cooling, the simulations were limited to multiples of three as the total number of reactor modules.

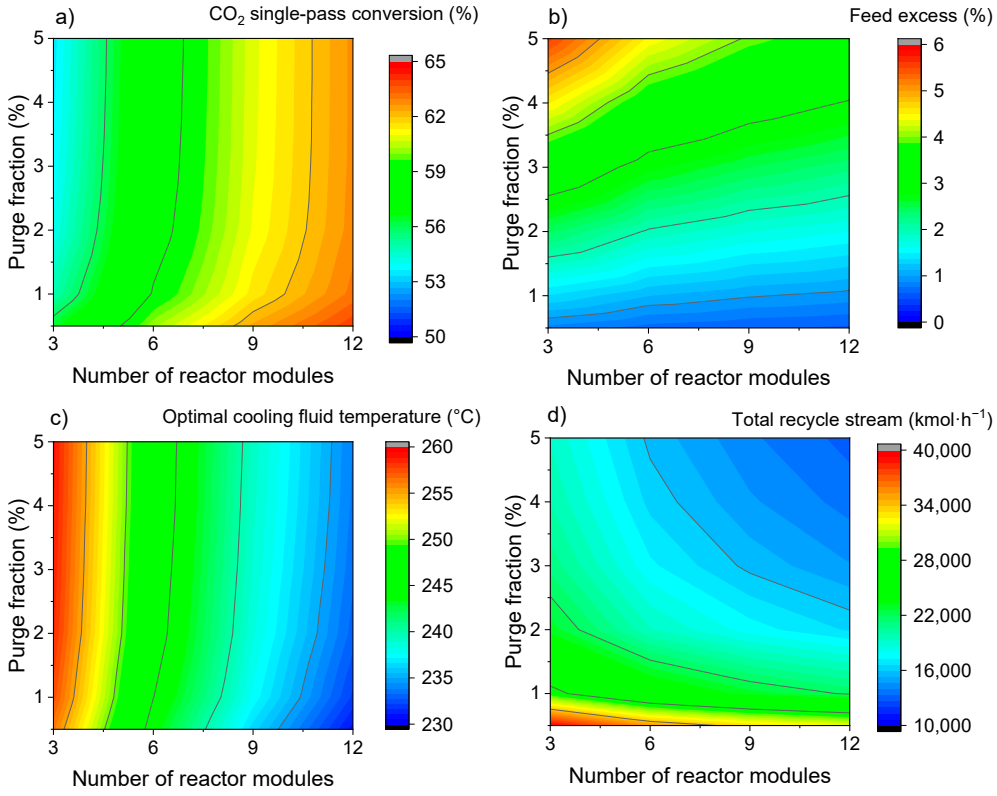

Figure 8. Three-step process—CO_2 single-pass conversion (**a**), required feed excess (**b**), optimal temperature (**c**), and total recycle stream (**d**) as a function of the number of reactor modules and the purge fraction.

A significant improvement was seen in the three-step process in relation to the one-step approach. For similar conditions (i.e., the same total number of reactor modules and purge stream fraction), CO_2 single-pass conversion had approximately doubled, the required feed excess decreased by 60–70%, and the total recycle stream decreased by 50–70%. The optimal values for the reactor cooling fluid remained close to the ones of the first approach (between 230 and 260 °C).

Similarly to the one-step process, a purge fraction equal to 2% was chosen here, having a good compromise between minimizing the feed requirements and minimizing the total recycle stream. With this fixed purge fraction, a number of reactor modules equal to three was selected, as further increasing this amount gave limited improvement in the required feed excess and the total recycle stream, while considerably increasing equipment and catalyst costs.

When analyzing different scenarios in Matlab, the same cooling fluid temperature (T_w) was considered for all reactors. A further optimization was possible by allowing this temperature to be independently operated in each reactor. This possibility was checked for the chosen condition (2% purge fraction, three reactor modules), but only a marginal improvement was obtained (see Table 3), probably not justifying the increase in plant complexity. Therefore, in the detailed analysis, the cooling fluid temperature of all the reactors was set to 258.5 °C.

Table 3. Three-step synthesis—Performance indicators for two process approaches: same cooling fluid temperature in all reactors, and independent optimization of the cooling fluid temperature in each reactor.

Approach	$T_{w,R1}$ (°C)	$T_{w,R2}$ (°C)	$T_{w,R3}$ (°C)	$X_{CO_2,SP}$ (%)	Feed Excess (%)	Total Recycle Stream (kmol·h^{-1})
Same T_w	258.5	258.5	258.5	54.1	2.42	23,038
Varying T_w	264.6	259.9	249.4	54.6	2.35	22,464

Similarly to the one-step process, the average heat transfer coefficients were obtained for each reactor and given to Aspen Plus: U_1 = 327 W·m^{-2}·K^{-1}, U_2 = 285 W·m^{-2}·K^{-1}, U_3 = 246 W·m^{-2}·K^{-1}. The decrease in the coefficient values is associated with a decrease in total flow, due to intermediate product removal. Still, the heat transfer coefficients were higher than in the one-step process (155 W·m^{-2}·K^{-1}), which had lower flows for each reactor module because of parallel operation.

3.2.2. Three-Step Process—Detailed Plant Simulation and Process Analysis

A detailed flowsheet of the three-step process presented in Figure 4 was implemented in Aspen Plus, considering a 2% purge fraction, three reactor modules working in series with intermediate product condensation, and the previously optimized temperature of the reactor cooling fluid (T_w = 258.5 °C). A detailed plant description, stream properties, and a picture of the flowsheet in Aspen Plus are provided in the Supplementary Material (Section F).

In Figure 9, the concentration of the products along the length of the three reactors is shown, as well as the product removal through the intermediate condensation steps. In Reactor 1, CO entered at a low concentration (1.3% mol/mol), peaked at z = 2.5 m, and left the reactor with a higher concentration (2.7% mol/mol). This CO production through the rWGSR increased the water concentration ($y_{H_2O}^{R_1,out}$ = 5.6% mol/mol) and slowed down methanol production ($y_{MeOH}^{R_1,out}$ = 4.7% mol/mol).

In Reactors 2 and 3, the CO inlet concentration was significantly higher (3.0% mol/mol for both cases), causing its concentration peak to come much sooner (at 1.8 m and 1.25 m, respectively). After that, the WGSR was faster than its reverse reaction and the CO concentration decreased, leaving both reactors with an overall positive CO consumption. Therefore, the water concentration in Reactors 2 and 3 was maintained at lower levels ($y_{H_2O}^{R_2,out}$ = 4.7% mol/mol, $y_{H_2O}^{R_3,out}$ = 4.5% mol/mol), enhancing the final methanol concentration ($y_{MeOH}^{R_2,out}$ = 5.6% mol/mol, $y_{MeOH}^{R_3,out}$ = 5.8% mol/mol).

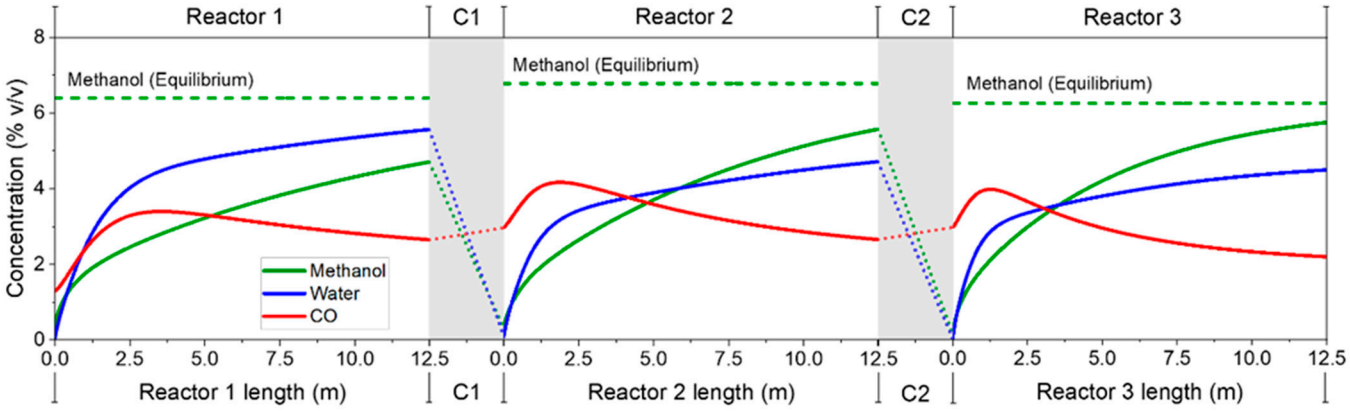

Figure 9. Three-step process—methanol, water, and CO concentration along the length of each reactor, as well as in the intermediate condensation steps (C1 and C2).

Water is known to accelerate the deactivation of Cu-based catalysts [67]. Therefore, the lower water concentration of the three-step process in relation to the one-step process ($y_{H_2O}^{1s,out}$ = 7.2%) should not only benefit the reaction rates, but also the catalyst lifetime.

In Table 4, the operating conditions and split ratios of the intermediate condensation steps are provided, while the reactor information is summarized in Table 5. Methanol and water were almost fully removed from the gas phase, but at the cost of ca. 9–13% CO_2 condensation. The split ratios of CO_2 and methanol were strongly dependent on temperature, with the chosen values (T_1 = 45 °C, T_2 = 30 °C) being derived from a sensitivity analysis.

Table 4. Three-step process—operating conditions and split ratios of the intermediate condensation steps.

Cond. Step	Temp. (°C)	Pres. (Bar)	Phase	Split Ratio CO_2 (%)	Split Ratio MeOH (%)	Split Ratio H_2O (%)
#1	45	69.25	Gas	90.66	5.31	1.17
			Liquid	9.34	94.69	98.83
#2	30	68.50	Gas	87.36	2.46	0.52
			Liquid	12.64	97.54	99.48

Table 5. Three-step process—heat transfer, inlet mole flow, mole fractions, and methanol production in the reactor modules.

Reactor	#1	#2	#3
$\dot{Q}$ (MW)	−18.5	−25.7	−22.7
$\dot{n}_{in}$ (kmol·h^{-1})	40,833	33,209	26,366
$y_{H_2,in}$ (% mol/mol)	69.1	69.0	69.5
$y_{CO,in}$ (% mol/mol)	1.3	3.0	3.0
$y_{CO_2,in}$ (% mol/mol)	20.6	17.3	14.4
$y_{MeOH,out}$ (% mol/mol)	4.7	5.6	5.8
$y_{H_2O,out}$ (% mol/mol)	5.6	4.7	4.5
$\Delta\dot{n}_{MeOH}$ (kmol·h^{-1})	1616	1589	1325

The methanol production was similar in Reactors 1 and 2 (1616 and 1589 kmol·h^{-1}, respectively), while it was 18% lower in Reactor 3 (1325 kmol·h^{-1}). This shows the positive effect of a higher CO concentration in the reactor feed, despite the lower total feed flow and CO_2 inlet concentration of Reactors 2 and 3 in relation to Reactor 1.

The CO_2 single-pass conversion ($X_{CO_2,SP}$) was 53.9%, with a selectivity to methanol of 99.8% and a selectivity to CO of 0.2%. The feed excess was 2.35%, leading to an overall conversion of CO_2 to methanol of 97.7%. These values are in agreement with the Matlab simulations ($X_{CO_2,SP}$ = 54.1%, Exc = 2.42%, overall CO_2 conversion to MeOH = 97.6%).

The three-step approach was significantly superior to the one-step process, even using only half the number of reactor modules (three vs. six). This superiority is clear when

looking at the CO_2 single-pass conversion (53.9% vs. 28.5%), leading to a considerably higher overall conversion to methanol (97.7% vs. 94.3%).

With the heat integration, the three-step process was also self-sufficient in heat, while electricity was produced through a water Rankine cycle, reducing the total power consumption from 42.7 to 21.8 MW. The chemical conversion efficiency was η_{CCE}^{3s} = 85.6%, which was higher than the value of the one-step process (η_{CCE}^{1s} = 82.3%) and, therefore, even closer to the maximum possible value ($\eta_{CCE,max}$ = 87.6%).

In Figure 10, an exergy analysis of the process is presented. The exergy efficiency was η_{Ex}^{3s} = 78.8%, an improvement from the previous approach (η_{Ex}^{1s} = 76.4%), with the total exergy losses decreasing in 13% (245.3 vs. 281.9 MW). Although the total power consumption decreased (42.7 vs. 47.4 MW), the net power consumption increased slightly (21.8 vs. 17.6 MW). This occurred because power generation was significantly lower in the three-step approach (20.8 vs. 29.8 MW) due to the much lower heat duty of the fired heater, as less reactant was lost in the purge streams.

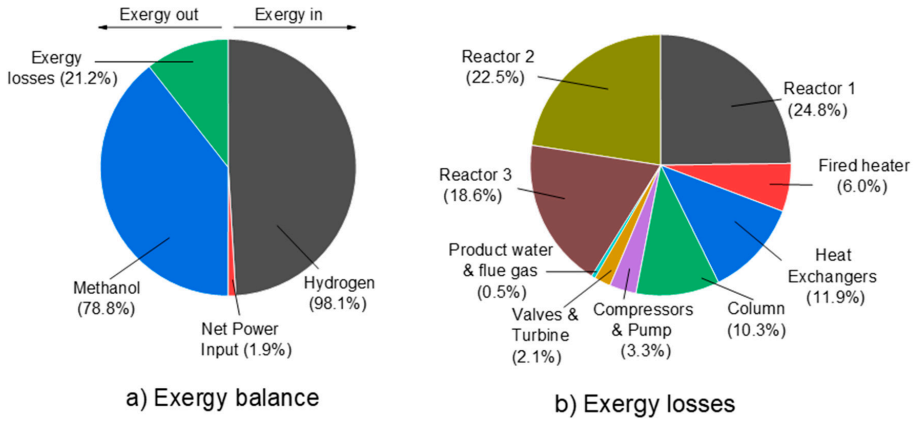

Figure 10. Three-step process—exergy analysis. (**a**) Global exergy balance (total exergy input = 1157.5 MW). (**b**) Distribution of exergy losses (total = 245.3 MW).

Chemical reactions with heat recovery at low temperatures was also the main cause of exergy losses in the three-step approach (reactor modules: 66.0%, fired heater: 6.0%). Both processes lost approximately the same exergy in the reactor modules and the distillation column. The main improvement in relation to the one-step process was a much lower exergy loss in the fired heater (14.7 vs. 41.4 MW), as the total purge stream flow decreased by 59% (455 against 1100 kmol·h^{-1}). Despite the higher number of cooling and warming operations and the higher total heat transfer duty in the three-step process (357.1 vs. 310.2 MW), the exergy losses in the heat exchangers were slightly lower for the three-step process (29.4 vs. 31.4 MW). Finally, moderate improvements were also seen in the compressors and pump (8.2 vs. 9.1 MW) and in the valves and turbine (5.0 vs. 7.4 MW).

In Table 6, the data comparing both processes is summarized, once again emphasizing the superior performance of the three-step approach.

Table 6. Data comparison between the one-step and the three-step approach.

Item	One-Step	Three-Step
Total methanol production (kmol·h^{-1})	4527	4525
CO_2 single-pass conversion (%)	28.5	53.9
Overall CO_2 conversion to methanol (%)	94.3	97.7
Feed excess (%)	6.05	2.35
Methanol selectivity (%)	99.5	99.8
Total recycle stream flow (kmol·h^{-1})	54,290	22,581
Maximum water concentration (% mol/mol)	7.2	5.6
Total exergy loss (MW)	281.9	245.3
Exergy efficiency (%)	76.4	78.8

3.3. Techno-Economic Analysis

In Figure 11a, the distribution of the equipment costs (EC) is presented, with the reactor modules and the compressors representing the majority of the costs (>75%). The total EC was 85.5 and 66.1 M€ for the one-step and the three-step approach, respectively. This significant improvement of the three-step process was a consequence of the intermediate condensation steps, requiring a lower total reactor volume (due to an enhanced reaction velocity), lower compressor size (due to a lower recycle flow), and lower furnace, turbine, and generator size (due to a lower purge flow). The cost reduction in the aforementioned equipment was significantly higher than the additional costs of the heat exchangers and flash drums from the intermediate condensation units. The total fixed capital investment (FCI) was 415.9 and 321.4 M€ for the one-step and three-step approach, respectively. The detailed estimated capacity and price of each equipment is presented in the Supplementary Material (Section H).

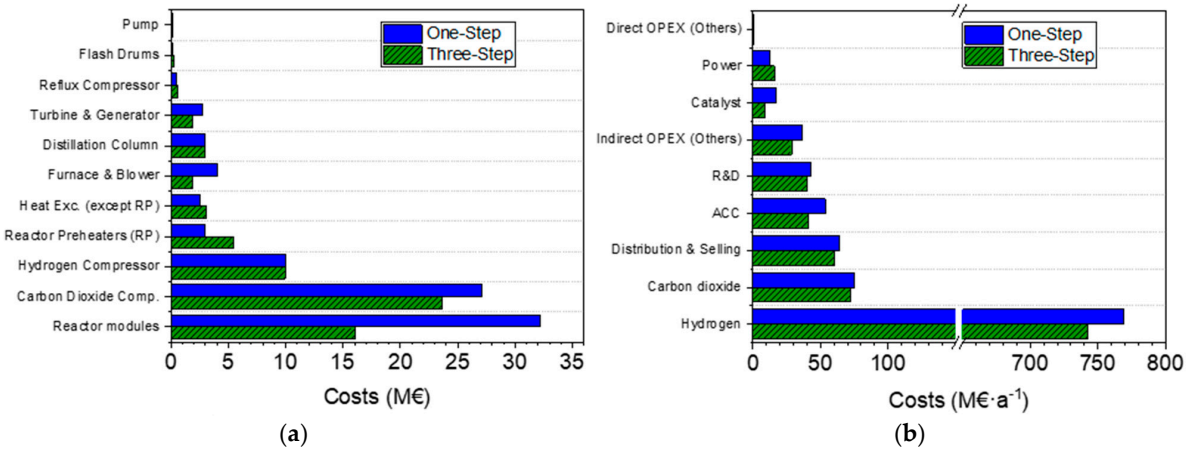

Figure 11. Distribution of the costs. (**a**) Equipment Costs (EC). (**b**) Net Production Costs (NPC).

In Figure 11b, the distribution of the net production costs (NPC) is detailed. The main operating costs were the reactant expenses (78–80% of NPC), with ACC contributing with only 4–5%, while the catalysts and electricity consisted of less than 3% of the NPC. Due to the higher overall CO_2 conversion to methanol, the NPC of the three-step process was 5.7% lower than the one-step approach. The detailed $OPEX$ costs are presented in the Supplementary Material (Section H).

In Table 7, a summary of the overall costs is presented. The NPC was 920 and 868 €·ton^{-1} for the one-step and the three-step process, respectively, corresponding to an improvement of 5.7% for the new process. Besides the hydrogen and carbon dioxide costs, the fixed capital investment (FCI) and the discount rate were the most sensitive parameters to the methanol selling price, as shown in the tornado analysis (see Figure 12).

Table 7. Summary of the costs of the one-step and the three-step process.

Item	Costs		Decrease (%)
	One-Step	Three-Step	
Equipment Costs (EC)	85.5 M€	66.1 M€	22.7
Fixed capital investment (FCI)	415.9 M€	321.4 M€	22.7
Working capital (WC)	46.2 M€	35.7 M€	22.7
Total $CAPEX$	462.1 M€	357.1 M€	22.7
Annual Capital Costs (ACC)	53.5 M€·a^{-1}	41.3 M€·a^{-1}	22.7
Direct $OPEX$	874.9 M€·a^{-1}	839.6 M€·a^{-1}	4.0
Indirect $OPEX$	143.4 M€·a^{-1}	129.6 M€·a^{-1}	9.6
Total $OPEX$	1018.3 M€·a^{-1}	969.3 M€·a^{-1}	4.8
Net Production Costs (NPC)	1071.8 M€·a^{-1}	1010.6 M€·a^{-1}	5.7

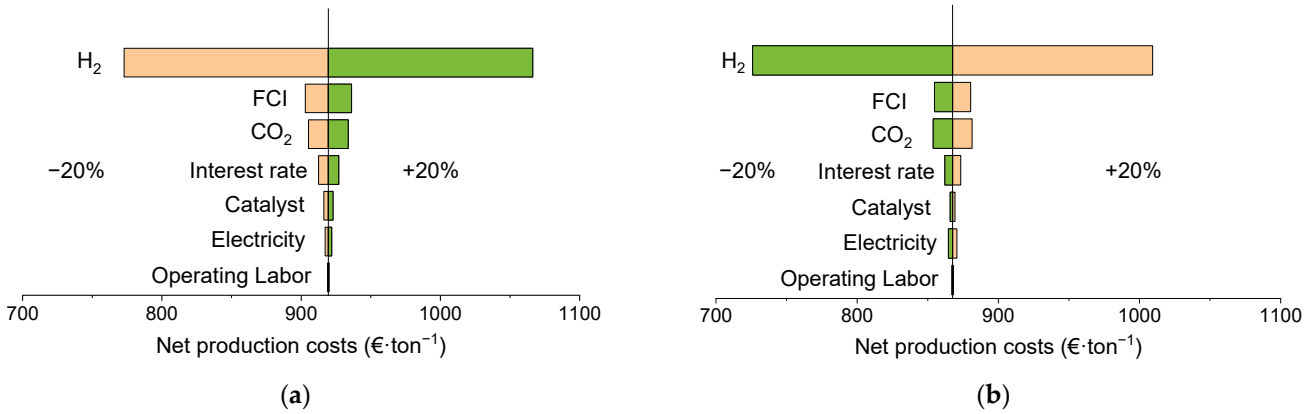

Figure 12. Sensitivity analysis of the main cost factors in relation to the net production costs (NPC). Variation of ± 20% in each factor. (**a**) One-step process. (**b**) Three-step process.

In Figure 13, the net production costs are plotted against the hydrogen price. Although the methanol market price in Europe was still significantly below the values (495 €·ton^{-1} in February 2022), [68,69] the green methanol produced from the proposed process would become economically competitive if the green hydrogen price reached 1468 €·ton^{-1}.

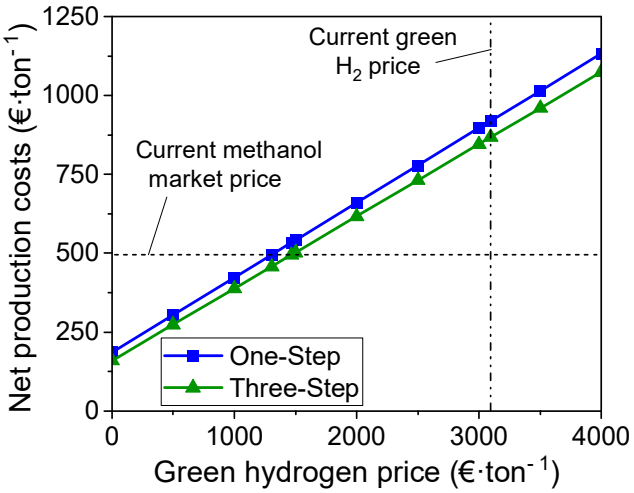

Figure 13. Net production costs of methanol as a function of green hydrogen price.

4. Conclusions

A detailed study of a methanol synthesis plant from H_2 and CO_2 with intermediate condensation units (the three-step process) is presented and compared with the conventional approach (the one-step process). The total production was fixed at 1.16 Mton MeOH·a^{-1}. The processes were first implemented in Matlab in order to critically analyze the number of reactor modules, the purge fraction, and the reactor operating temperature. Using the most suitable process parameters, detailed plants of both approaches were implemented in Aspen Plus, including heat integration and a water Rankine cycle to make use of the reaction enthalpy. Finally, techno-economic analyses were applied. Both processes offered an excess of heat, which was used to generate electricity in our work, but could alternatively supply other plants (e.g., CCU, OME synthesis) in a larger process integration.

It was demonstrated that CO_2 single-pass conversion almost doubled when including intermediate condensation steps (53.9 vs. 28.5%), resulting in a significantly higher overall conversion to methanol (97.7 vs. 94.3%) and in a higher exergy efficiency (78.8 vs. 76.4%). Because of the enhanced conversion, the new process required lower recycle and feed streams, decreasing net production costs by 61.2 M€·a^{-1} (5.7%). Although additional equipment (i.e., heat exchangers and gas–liquid separators) is necessary, the improved

process was significantly more efficient than the conventional approach, requiring lower sizes of the main equipment (e.g., compressors, reactors, fired heater). Consequently, according to our analysis, the total investment costs were 94.5 M€ (22.7%) lower than for the conventional process.

Intermediate condensation steps are therefore highly recommended for methanol production from H_2/CO_2, reducing costs by improving CO_2 equilibrium conversion to methanol while using commercially proven technology. Besides, since water accelerates the deactivation of Cu-based catalysts, product intermediate removal should increase catalyst lifetime, as the average water concentration in the reactor is significantly lower than in the conventional process.

With our proposed process, the methanol net production costs amounted to 868 €·ton^{-1}, which are still significantly higher than the current market price (495 €·ton^{-1}) but is believed to become economically viable with an effective reduction in the price of green hydrogen.

Supplementary Materials: The following supporting information can be downloaded at: https://www.mdpi.com/article/10.3390/pr10081535/s1, Figure S1: One-step process—Aspen Plus flowsheet; Figure S2: Three-step process—Aspen Plus flowsheet; Table S1: Parameters for the estimation of the specific heat capacity and specific enthalpy of selected components in the gas phase; Table S2: Liquid and gas fractions (% mol/mol) of the phase separation via flash drums and the separation via the distillation column in the one-step process. Values taken from Aspen Plus calculations and used for the Matlab simulations; Table S3: Liquid and gas fractions (% mol/mol) of the phase separation via flash drums and the separation via the distillation column in the three-step process. Values taken from Aspen Plus calculations and used for the Matlab simulations; Table S4: Aspen kinetic factor and Model-6p corresponding expressions; Table S5: Coefficients of the driving force constant and the corresponding expressions from Model-6p; Table S6: Concentration exponents (v_j) of the driving force expression; Table S7: Adsorption constants and the corresponding expression of Model-6p; Table S8: Concentration exponents and the corresponding values of Model-6p; Table S9: Properties of the streams from the one-step process; Table S10: Molar composition (% mol/mol) of the streams from the one-step process; Table S11: Properties of the streams from the three-step process; Table S12: Molar composition (% mol/mol) of the streams from the three-step process; Table S13: Dimension of the flash drums of the one-step and the three-step processes; Table S14: Global heat transfer coefficients, heat transfer duty, and estimated surface area of the heat exchangers of the one-step and the three-step process; Table S15: Calculation of the Capital Expenses (CAPEX) depending on the total equipment costs (EC); Table S16: Estimation of indirect operating expenses ($OPEX_{ind}$); Table S17: Equipment characteristic dimensions and equipment costs (EC) of the one-step approach. All equipment was built with carbon steel. All equipment reference prices were taken from Peters et al., except for the power generator, whose ref. price was taken from Henning and Haase; Table S18: Equipment characteristic dimensions and equipment costs (EC) of the three-step approach. All equipment was built with carbon steel, and the costs included 10% delivery costs. All equipment reference prices were taken from Peters et al., except for the power generator, whose ref. price was taken from Henning and Haase; Table S19: Detailed operating expenditures (OPEX) of the one-step and the three-step approach.

Author Contributions: Conceptualization, B.L.d.O.C. and J.S.; methodology, B.L.d.O.C., K.J. and P.B.; software, B.L.d.O.C., K.J. and P.B.; formal analysis, B.L.d.O.C.; writing—original draft preparation, B.L.d.O.C.; writing—review and editing, K.J., P.B., K.H.D., S.P., N.D. and J.S.; visualization, B.L.d.O.C. and P.B.; supervision, K.H.D., S.P., N.D. and J.S.; funding acquisition, K.H.D., S.P., and J.S. All authors have read and agreed to the published version of the manuscript.

Funding: This research was funded by Coordenação de Aperfeiçoamento de Pessoal de Nível Superior (CAPES) (process number: 88881.174609/2018-01) and by the Helmholtz Research Program "Materials and Technologies for the Energy Transition (MTET), Topic 3: Chemical Energy Carriers". We also acknowledge the support from the KIT-Publication Fund of the Karlsruhe Institute of Technology.

Conflicts of Interest: The authors declare no conflict of interest. The funders had no role in the design of the study; in the collection, analyses, or interpretation of data; in the writing of the manuscript; or in the decision to publish the results.

References

1. Our World in Data. Renewable Energy. Available online: https://ourworldindata.org/renewable-energy (accessed on 4 April 2022).
2. Daiyan, R.; MacGill, I.; Amal, R. Opportunities and challenges for renewable power-to-X. *ACS Energy Lett.* **2020**, *5*, 3843–3847. [CrossRef]
3. Younas, M.; Shafique, S.; Hafeez, A.; Javed, F.; Rehman, F. An overview of hydrogen production: Current status, potential, and challenges. *Fuel* **2022**, *316*, 123317. [CrossRef]
4. Chisholm, G.; Zhao, T.; Cronin, L. 24—Hydrogen from water electrolysis. In *Storing Energy*, 2nd ed.; Letcher, T.M., Ed.; Elsevier: Amsterdam, The Netherlands, 2022; pp. 559–591. [CrossRef]
5. Artz, J.; Müller, T.E.; Thenert, K.; Kleinekorte, J.; Meys, R.; Sternberg, A.; Bardow, A.; Leitner, W. Sustainable conversion of carbon dioxide: An integrated review of catalysis and life cycle assessment. *Chem. Rev.* **2018**, *118*, 434–504. [CrossRef] [PubMed]
6. Wang, L.; Chen, M.; Küngas, R.; Lin, T.-E.; Diethelm, S.; Maréchal, F.; Van Herle, J. Power-to-fuels via solid-oxide electrolyzer: Operating window and techno-economics. *Renew. Sustain. Energy Rev.* **2019**, *110*, 174–187. [CrossRef]
7. Bongartz, D.; Burre, J.; Ziegler, A.L.; Mitsos, A. Power-to-OME1 via direct oxidation of methanol: Process design and global flowsheet optimization. In *Computer Aided Chemical Engineering*; Türkay, M., Gani, R., Eds.; Elsevier: Amsterdam, The Netherlands, 2021; Volume 50, pp. 273–278.
8. Schmidt, P.; Batteiger, V.; Roth, A.; Weindorf, W.; Raksha, T. Power-to-liquids as renewable fuel option for aviation: A review. *Chem. Ing. Tech.* **2018**, *90*, 127–140. [CrossRef]
9. Methanol Institute—Methanol Fuel in China 2020. Available online: https://www.methanol.org/methanol-fuel-in-china-full-report/ (accessed on 5 July 2022).
10. Global Data—Methanol Market Capacity 2021. Available online: https://www.globaldata.com/store/report/methanol-market-analysis/ (accessed on 27 June 2022).
11. Bozzano, G.; Manenti, F. Efficient methanol synthesis: Perspectives, technologies and optimization strategies. *Prog. Energy Combust. Sci.* **2016**, *56*, 71–105. [CrossRef]
12. Freepik. Flaticon Icons. Available online: https://www.flaticon.com/authors/freepik (accessed on 27 June 2022).
13. Ott, J.; Gronemann, V.; Pontzen, F.; Fiedler, E.; Grossmann, G.; Kersebohm, D.B.; Weiss, G.; Witte, C. Methanol. In *Ullmann's Encyclopedia of Industrial Chemistry*; Wiley: New York, NY, USA, 2012. [CrossRef]
14. Toyo Engineering. G-Methanol. Available online: https://www.toyo-eng.com/jp/en/solution/g-methanol/ (accessed on 9 May 2022).
15. Lacerda de Oliveira Campos, B.; Herrera Delgado, K.; Wild, S.; Studt, F.; Pitter, S.; Sauer, J. Surface reaction kinetics of the methanol synthesis and the water gas shift reaction on $Cu/ZnO/Al_2O_3$. *React. Chem. Eng.* **2021**, *6*, 868–887. [CrossRef]
16. Studt, F.; Behrens, M.; Kunkes, E.L.; Thomas, N.; Zander, S.; Tarasov, A.; Schumann, J.; Frei, E.; Varley, J.B.; Abild-Pedersen, F.; et al. The mechanism of CO and CO_2 hydrogenation to methanol over Cu-based catalysts. *ChemCatChem* **2015**, *7*, 1105–1111. [CrossRef]
17. Bussche, K.M.V.; Froment, G.F. A steady-state kinetic model for methanol synthesis and the water gas shift reaction on a commercial $Cu/ZnO/Al_2O_3$Catalyst. *J. Catal.* **1996**, *161*, 1–10. [CrossRef]
18. Slotboom, Y.; Bos, M.J.; Pieper, J.; Vrieswijk, V.; Likozar, B.; Kersten, S.R.A.; Brilman, D.W.F. Critical assessment of steady-state kinetic models for the synthesis of methanol over an industrial $Cu/ZnO/Al_2O_3$ catalyst. *Chem. Eng. J.* **2020**, *389*, 124181. [CrossRef]
19. Lacerda de Oliveira Campos, B.; Herrera Delgado, K.; Pitter, S.; Sauer, J. Development of consistent kinetic models derived from a microkinetic model of the methanol synthesis. *Ind. Eng. Chem. Res.* **2021**, *60*, 15074–15086. [CrossRef]
20. Pérez-Fortes, M.; Schöneberger, J.C.; Boulamanti, A.; Tzimas, E. Methanol synthesis using captured CO_2 as raw material: Techno-economic and environmental assessment. *Appl. Energy* **2016**, *161*, 718–732. [CrossRef]
21. Szima, S.; Cormos, C.-C. Improving methanol synthesis from carbon-free H_2 and captured CO_2: A techno-economic and environmental evaluation. *J. CO_2 Util.* **2018**, *24*, 555–563. [CrossRef]
22. Cordero-Lanzac, T.; Ramirez, A.; Navajas, A.; Gevers, L.; Brunialti, S.; Gandía, L.M.; Aguayo, A.T.; Mani Sarathy, S.; Gascon, J. A techno-economic and life cycle assessment for the production of green methanol from CO_2: Catalyst and process bottlenecks. *J. Energy Chem.* **2022**, *68*, 255–266. [CrossRef]
23. FFE München. Electrolysis, the Key Technology for Power-to-X. Available online: https://www.ffe.de/veroeffentlichungen/elektrolyse-die-schluesseltechnologie-fuer-power-to-x/ (accessed on 4 April 2022).
24. Fasihi, M.; Efimova, O.; Breyer, C. Techno-economic assessment of CO_2 direct air capture plants. *J. Clean. Prod.* **2019**, *224*, 957–980. [CrossRef]
25. Carbon Recycling International. Renewable Methanol from Carbon Dioxide. Available online: https://www.carbonrecycling.is/ (accessed on 4 April 2022).
26. Siemens Energy. The Haru Oni Hydrogen Plant. Available online: https://www.siemens-energy.com/global/en/news/magazine/2021/haru-oni.html (accessed on 1 February 2022).
27. van Bennekom, J.G.; Venderbosch, R.H.; Winkelman, J.G.M.; Wilbers, E.; Assink, D.; Lemmens, K.P.J.; Heeres, H.J. Methanol synthesis beyond chemical equilibrium. *Chem. Eng. Sci.* **2013**, *87*, 204–208. [CrossRef]
28. Bos, M.J.; Brilman, D.W.F. A novel condensation reactor for efficient CO_2 to methanol conversion for storage of renewable electric energy. *Chem. Eng. J.* **2015**, *278*, 527–532. [CrossRef]

29. Seshimo, M.; Liu, B.; Lee, H.R.; Yogo, K.; Yamaguchi, Y.; Shigaki, N.; Mogi, Y.; Kita, H.; Nakao, S.-i. Membrane reactor for methanol synthesis using Si-Rich LTA Zeolite Membrane. *Membranes* **2021**, *11*, 505. [CrossRef]
30. Johnson Mattey. Methanol Synthesis Technology. Available online: https://matthey.com/en/products-and-services/chemical-processes/core-technologies/synthesis (accessed on 9 May 2022).
31. Guo, Y.; Li, G.; Zhou, J.; Liu, Y. Comparison between hydrogen production by alkaline water electrolysis and hydrogen production by PEM electrolysis. *IOP Conf. Ser. Earth Environ. Sci.* **2019**, *371*, 042022. [CrossRef]
32. Porter, R.T.J.; Fairweather, M.; Kolster, C.; Mac Dowell, N.; Shah, N.; Woolley, R.M. Cost and performance of some carbon capture technology options for producing different quality CO_2 product streams. *Int. J. Greenh. Gas Control.* **2017**, *57*, 185–195. [CrossRef]
33. Bennekom, J.G.v.; Winkelman, J.G.M.; Venderbosch, R.H.; Nieland, S.D.G.B.; Heeres, H.J. Modeling and experimental studies on phase and chemical equilibria in high-pressure methanol synthesis. *Ind. Eng. Chem. Res.* **2012**, *51*, 12233–12243. [CrossRef]
34. Gaikwad, R.; Bansode, A.; Urakawa, A. High-pressure advantages in stoichiometric hydrogenation of carbon dioxide to methanol. *J. Catal.* **2016**, *343*, 127–132. [CrossRef]
35. Süd-Chemie AG. Safety Data Sheet—MegaMax 700. 2006.
36. Zhu, J.; Araya, S.S.; Cui, X.; Sahlin, S.L.; Kær, S.K. Modeling and design of a multi-tubular packed-bed reactor for methanol steam reforming over a $Cu/ZnO/Al_2O_3$ Catalyst. *Energies* **2020**, *13*, 610. [CrossRef]
37. Van-Dal, É.S.; Bouallou, C. Design and simulation of a methanol production plant from CO_2 hydrogenation. *J. Clean. Prod.* **2013**, *57*, 38–45. [CrossRef]
38. Pontzen, F.; Liebner, W.; Gronemann, V.; Rothaemel, M.; Ahlers, B. CO_2-based methanol and DME—Efficient technologies for industrial scale production. *Catal. Today* **2011**, *171*, 242–250. [CrossRef]
39. Bongartz, D.; Burre, J.; Mitsos, A. Production of oxymethylene dimethyl ethers from hydrogen and carbon dioxide—Part I: Modeling and analysis for OME1. *Ind. Eng. Chem. Res.* **2019**, *58*, 4881–4889. [CrossRef]
40. Burners for Fired Heaters in General Refinery Services. In *Reference Practice (RP) 535*, 3rd ed.; American Petroleum Institute (API): Washington, DC, USA, 2014.
41. Goos, E.; Burcat, A.; Ruscic, B. New NASA Thermodynamic Polynomials Database. Available online: http://garfield.chem.elte.hu/Burcat/THERM.DAT (accessed on 4 March 2022).
42. Gruber, M. Detaillierte Untersuchung des Wärme und Stofftransports in einem Festbett-Methanisierungsreaktor für Power-to-Gas Anwendungen. Ph.D. Thesis, Karlsruhe Institute of Technology (KIT), Karlsruhe, Germany, 2019; 275p.
43. *VDI Heat Atlas*, 2nd ed.; Springer: Berlin-Heidelberg, Germany, 2010; p. 1585.
44. Seidel, C.; Jörke, A.; Vollbrecht, B.; Seidel-Morgenstern, A.; Kienle, A. Kinetic modeling of methanol synthesis from renewable resources. *Chem. Eng. Sci.* **2018**, *175*, 130–138. [CrossRef]
45. Peng, D.-Y.; Robinson, D.B. A new two-constant equation of State. *Ind. Eng. Chem. Fundam.* **1976**, *15*, 59–64. [CrossRef]
46. Meng, L.; Duan, Y.-Y.; Wang, X.-D. Binary interaction parameter kij for calculating the second cross-virial coefficients of mixtures. *Fluid Phase Equilibria* **2007**, *260*, 354–358. [CrossRef]
47. Meng, L.; Duan, Y.-Y. Prediction of the second cross virial coefficients of nonpolar binary mixtures. *Fluid Phase Equilibria* **2005**, *238*, 229–238. [CrossRef]
48. Deiters, U.K. Comments on the modeling of hydrogen and hydrogen-containing mixtures with cubic equations of state. *Fluid Phase Equilibria* **2013**, *352*, 93–96. [CrossRef]
49. Kuld, S.; Thorhauge, M.; Falsig, H.; Elkjær, C.F.; Helveg, S.; Chorkendorff, I.; Sehested, J. Quantifying the promotion of Cu catalysts by ZnO for methanol synthesis. *Science* **2016**, *352*, 969–974. [CrossRef] [PubMed]
50. CLARIANT. Catalysts for Methanol Synthesis, Product Data Sheet. 2017. Available online: https://www.clariant.com/-/media/Files/Solutions/Products/Additional-Files/M/18/Clariant-Brochure-Methanol-Synthesis-201711-EN.pdf (accessed on 4 April 2022).
51. Saito, M.; Murata, K. Development of high performance Cu/ZnO-based catalysts for methanol synthesis and the water-gas shift reaction. *Catal. Surv. Asia* **2004**, *8*, 285–294. [CrossRef]
52. Campos Fraga, M.M.; Lacerda de Oliveira Campos, B.; Lisboa, M.S.; Almeida, T.B.; Costa, A.O.S.; Lins, V.F.C. Analysis of a Brazilian thermal plant operation applying energetic and exergetic balances. *Braz. J. Chem. Eng.* **2018**, *35*, 1395–1403. [CrossRef]
53. Nitzsche, R.; Budzinski, M.; Gröngröft, A. Techno-economic assessment of a wood-based biorefinery concept for the production of polymer-grade ethylene, organosolv lignin and fuel. *Bioresour. Technol.* **2016**, *200*, 928–939. [CrossRef] [PubMed]
54. Green, D.W.; Southard, M.Z. *Perry's Chemical Engineers' Handbook*, 9th ed.; McGraw Hill: New York, NY, USA, 2018.
55. König, D.H.; Baucks, N.; Dietrich, R.-U.; Wörner, A. Simulation and evaluation of a process concept for the generation of synthetic fuel from CO_2 and H_2. *Energy* **2015**, *91*, 833–841. [CrossRef]
56. Albrecht, F.G.; König, D.H.; Baucks, N.; Dietrich, R.-U. A standardized methodology for the techno-economic evaluation of alternative fuels—A case study. *Fuel* **2017**, *194*, 511–526. [CrossRef]
57. Peters, M.S.; Timmerhaus, K.D.; West, R.E. *Plant Design and Economics for Chemical Engineers*, 5th ed.; McGraw-Hill Education Ltd.: Boston, MA, USA, 2002; p. 1008.
58. Hennig, M.; Haase, M. Techno-economic analysis of hydrogen enhanced methanol to gasoline process from biomass-derived synthesis gas. *Fuel Processing Technol.* **2021**, *216*, 106776. [CrossRef]
59. Travelex. Worldwide Money. Available online: https://www.travelex.com/currency/currency-pairs/usd-to-eur (accessed on 4 April 2022).

60. Towler, G.; Sinnott, R. *Chemical Engineering Design—Principles, Practice and Economics of Plant and Process Design*, 2nd ed.; Elsevier: Amsterdam, The Netherlands, 2013.
61. Aden, A.; Ruth, M.; Ibsen, K.; Jechura, J.; Neeves, K.; Sheehan, J.; Wallace, B.; Montague, L.; Slayton, A.; Lukas, J. *Lignocellulosic Biomass to Ethanol Process Design and Economics Utilizing Co-Current Dilute Acid Prehydrolysis and Enzymatic Hydrolysis for Corn Stover*; National Renewable Energy Laboratory: Golden, CO, USA, 2002; 154p.
62. Cheremisinoff, N.P. *Clean Electricity Through Advanced Coal Technologies*; Elsevier: Amsterdam, The Netherlands, 2012. [CrossRef]
63. Bustillo-Lecompte, C.F.; Mehrvar, M.; Quiñones-Bolaños, E. Cost-effectiveness analysis of TOC removal from slaughterhouse wastewater using combined anaerobic–aerobic and UV/H_2O_2 processes. *J. Environ. Manag.* **2014**, *134*, 145–152. [CrossRef]
64. Tan, E.C.; Talmadge, M.; Dutta, A.; Hensley, J.; Snowden-Swan, L.J.; Humbird, D.; Schaidle, J.; Biddy, M. Conceptual process design and economics for the production of high-octane gasoline blendstock via indirect liquefaction of biomass through methanol/dimethyl ether intermediates. *Biofuels Bioprod. Biorefining* **2016**, *10*, 17–35. [CrossRef]
65. Ashraf, M.T.; Schmidt, J.E. Process simulation and economic assessment of hydrothermal pretreatment and enzymatic hydrolysis of multi-feedstock lignocellulose—Separate vs. combined processing. *Bioresour. Technol.* **2018**, *249*, 835–843. [CrossRef] [PubMed]
66. Granjo, J.F.O.; Oliveira, N.M.C. Process simulation and techno-economic analysis of the production of sodium methoxide. *Ind. Eng. Chem. Res.* **2016**, *55*, 156–167. [CrossRef]
67. Prašnikar, A.; Pavlišič, A.; Ruiz-Zepeda, F.; Kovač, J.; Likozar, B. Mechanisms of copper-based catalyst deactivation during CO_2 reduction to methanol. *Ind. Eng. Chem. Res.* **2019**, *58*, 13021–13029. [CrossRef]
68. Argus Media. European Methanol Spot and Contract Prices. Available online: https://www.argusmedia.com/en/blog/2022/february/4/european-methanol-spot-and-contract-prices (accessed on 4 April 2022).
69. Methanol Institute—Methanol Prices, Supply and Demand. Available online: https://www.methanol.org/methanol-price-supply-demand/ (accessed on 4 April 2022).